


The W2020 Database of Validated Rovibrational Experimental Transitions and Empirical Energy Levels of Water Isotopologues. II. H₂¹⁷O and H₂¹⁸O with an Update to H₂¹⁶O

Cite as: J. Phys. Chem. Ref. Data **49**, 043103 (2020); <https://doi.org/10.1063/5.0030680>

Submitted: 23 September 2020 . Accepted: 16 November 2020 . Published Online: 30 December 2020

 Tibor Furtenbacher,  Roland Tóbiás,  Jonathan Tennyson, Oleg L. Polyansky, Aleksandra A. Kyuberis, Roman I. Ovsyannikov, Nikolay F. Zobov, and  Attila G. Császár

COLLECTIONS

 This paper was selected as Featured



View Online



Export Citation



CrossMark

ARTICLES YOU MAY BE INTERESTED IN

[W2020: A Database of Validated Rovibrational Experimental Transitions and Empirical Energy Levels of H₂¹⁶O](#)

Journal of Physical and Chemical Reference Data **49**, 033101 (2020); <https://doi.org/10.1063/5.0008253>

[A method of flight path and chirp pattern reconstruction for multiple flying bats](#)
Acoustics Research Letters Online **6**, 257 (2005); <https://doi.org/10.1121/1.2046567>

[Sun glints and luminous wriggles by the seashore](#)
American Journal of Physics **89**, 21 (2021); <https://doi.org/10.1119/10.0001882>



The W2020 Database of Validated Rovibrational Experimental Transitions and Empirical Energy Levels of Water Isotopologues. II. H_2^{17}O and H_2^{18}O with an Update to H_2^{16}O

Cite as: J. Phys. Chem. Ref. Data 49, 043103 (2020); doi: 10.1063/5.0030680

Submitted: 23 September 2020 • Accepted: 16 November 2020 •

Published Online: 30 December 2020



View Online



Export Citation



CrossMark

Tibor Furtenbacher,¹ Roland Tóbiás,¹ Jonathan Tennyson,² Oleg L. Polyansky,^{2,3} Aleksandra A. Kyuberis,⁴ Roman I. Ovsyannikov,³ Nikolay F. Zobov,³ and Attila G. Császár^{5,a)}

AFFILIATIONS

¹MTA-ELTE Complex Chemical Systems Research Group, P.O. Box 32, H-1518 Budapest, Hungary

²Department of Physics and Astronomy, University College London, Gower Street, London WC1E 6BT, United Kingdom

³Institute of Applied Physics, Russian Academy of Science, Ulyanov Street 46, Nizhny Novgorod 603950, Russia

⁴Van Swinderen Institute for Particle Physics and Gravity, University of Groningen, Nijenborgh 4, 9747 Groningen, The Netherlands

⁵Institute of Chemistry, ELTE Eötvös Loránd University, Pázmány sétány 1/A, H-1117 Budapest, Hungary and MTA-ELTE Complex Chemical Systems Research Group, P.O. Box 32, H-1518 Budapest, Hungary

^{a)} Author to whom correspondence should be addressed: csaszarag@caesar.elte.hu

ABSTRACT

The W2020 database of validated experimental transitions and accurate empirical energy levels of water isotopologues, introduced in the work of Furtenbacher *et al.* [J. Phys. Chem. Ref. Data **49**, 033101 (2020)], is updated for H_2^{16}O and newly populated with data for H_2^{17}O and H_2^{18}O . The $\text{H}_2^{17}\text{O}/\text{H}_2^{18}\text{O}$ spectroscopic data utilized in this study are collected from 65/87 sources, with the sources arranged into 76/99 segments, and the data in these segments yield 27 045/66 166 (mostly measured) rovibrational transitions and 5278/6865 empirical energy levels with appropriate uncertainties. Treatment and validation of the collated transitions of H_2^{16}O , H_2^{17}O , and H_2^{18}O utilized the latest, XML-based version of the MARVEL (Measured Active Rotational-Vibrational Energy Levels) protocol and code, called xMARVEL. The empirical rovibrational energy levels of H_2^{17}O and H_2^{18}O form a complete set through 3204 cm^{-1} and 4031 cm^{-1} , respectively. Vibrational band origins are reported for 37 and 52 states of H_2^{17}O and H_2^{18}O , respectively. The spectroscopic data of this study extend and improve the data collated by an International Union of Pure and Applied Chemistry Task Group in 2010 [J. Tennyson *et al.*, J. Quant. Spectrosc. Radiat. Transfer **110**, 2160 (2010)] as well as those reported in the HITRAN2016 information system. Following a minor but significant update to the W2020- H_2^{16}O dataset, the joint analysis of the rovibrational levels for the series H_2^{16}O , H_2^{17}O , and H_2^{18}O facilitated development of a consistent set of labels among these three water isotopologues and the provision of accurate predictions of yet to be observed energy levels for the minor isotopologues using the combination of xMARVEL results and accurate variational nuclear-motion calculations. To this end, 9925/8409 pseudo-experimental levels have been derived for $\text{H}_2^{17}\text{O}/\text{H}_2^{18}\text{O}$, significantly improving the coverage of accurate lines for these two minor water isotopologues up to the visible region. The W2020 database now contains almost all of the transitions, apart from those of HD^{16}O , required for a successful spectroscopic modeling of atmospheric water vapor.

© 2020 Author(s). All article content, except where otherwise noted, is licensed under a Creative Commons Attribution (CC BY) license (<http://creativecommons.org/licenses/by/4.0/>). <https://doi.org/10.1063/5.0030680>

CONTENTS

1. Introduction	2	2.2. The xMARVEL procedure	3
2. Methods and Data Treatment	3	2.3. Notation	4
2.1. Spectroscopic networks	3	2.4. Pseudo-experimental rovibrational levels	4
		3. The W2020 Datasets	4
		3.1. H_2^{16}O	4

3.2. H ₂ ¹⁷ O and H ₂ ¹⁸ O	6
4. Vibrational Band Origins	8
5. Validation of the W2020 Database Entries	11
6. Pseudo-experimental Rovibrational Levels	13
7. Comparison with HITRAN2016	13
8. Quadrupole-Allowed Transitions	14
9. Assessment of the Lamb-Dip Data of 10GaFaCaMa	14
10. Guiding Atmospheric Simulations	16
11. Summary and Conclusions	18
12. Supplementary Material	19
Acknowledgments	19
13. Data Availability	20
14. References	20

List of Tables

1. Data source segments and their characteristics for the H ₂ ¹⁷ O molecule	7
2. Data source segments and their characteristics for the H ₂ ¹⁸ O molecule	9
3. VBOs within the W2020-H ₂ ¹⁷ O dataset	11
4. VBOs within the W2020-H ₂ ¹⁸ O dataset	11
5. Comparison of the PE energies with their xMARVEL counterparts	14
6. Comparison of quadrupole-allowed transitions of H ₂ ¹⁶ O reported in 20CaKaYaKy ¹⁵² and 20CaSoSoYa ¹⁵³ with their xMARVEL counterparts	15
7. Comparison of the 10GaFaCaMa lines to their xMARVEL counterparts for H ₂ ¹⁸ O	16
8. Energy separation between selected pairs of pure rotational levels of H ₂ ¹⁸ O	16
9. Number of FP (Ref. 156 for H ₂ ¹⁶ O and HotWat78 ¹²⁸ for H ₂ ¹⁷ O and H ₂ ¹⁸ O), xMARVEL, and PE transitions of three water isotopologues, with different intensity cutoff values in cm molecule ⁻¹	17

List of Figures

1. Unsigned deviations of the 20MiKaMoCa ⁶⁶ lines from their W2020-H ₂ ¹⁶ O counterparts	5
---	---

1. Introduction

During the last century, one could witness outstanding research activity, yielding several hundred scientific papers, on the laboratory determination of rovibrational transitions of water isotopologues in the gas phase. This activity has been fueled largely by the considerable need for accurate line-by-line water data required by a number of scientific and engineering applications.^{1–4} The experimental studies have been aided by the appearance of new high-resolution and precision spectroscopic techniques^{5–12} as well as by the outstanding developments in the theory of (ultra)high-resolution spectroscopy.^{13–15} Most of the relevant spectroscopic data on water isotopologues available then were collected, cited, and analyzed in Refs. 16–20, detailing the work of a Task Group (TG) formed by the International Union of Pure and Applied Chemistry (IUPAC) on “A Database of Water Transitions from Experiment and

2. Unsigned deviations of the SISAM ¹⁵⁴ lines from their updated W2020-H ₂ ¹⁶ O counterparts	5
3. Differences between the H ₂ ¹⁶ O and H ₂ ¹⁸ O rovibrational energies for the vibrational bands of the $P = 5$ polyad at $J = 5$	6
4. Unsigned deviations of the SISAM ¹⁵⁴ states from their W2020-H ₂ ¹⁷ O counterparts	12
5. Unsigned deviations of the SISAM ¹⁵⁴ states from their W2020-H ₂ ¹⁸ O counterparts	12
6. Unsigned deviations of the HotWat78 ¹²⁸ energies from their W2020-H ₂ ¹⁷ O counterparts	12
7. Unsigned deviations of the HotWat78 ¹²⁸ energies from their W2020-H ₂ ¹⁸ O counterparts	12
8. Unsigned deviations of the 20MiKaMoCa ⁶⁶ lines from their W2020-H ₂ ¹⁷ O counterparts	13
9. Unsigned deviations of the 20MiKaMoCa ⁶⁶ lines from their W2020-H ₂ ¹⁸ O counterparts	13
10. Pictorial representation of all the non-isolated precision measurements performed for <i>ortho</i> - [panel (a)] and <i>para</i> -H ₂ ¹⁸ O [panel (b)]	15
11. Room-temperature ($T = 296$ K), one-photon, dipole-allowed H ₂ ¹⁶ O linelist up to 30 000 cm ⁻¹ , with an intensity cutoff of 10 ⁻²⁶ cm molecule ⁻¹ , based on xMARVEL line positions and PoKaZaTeL ¹⁵⁶ line positions	17
12. Room-temperature one-photon, dipole-allowed H ₂ ¹⁷ O linelist up to 14 000 cm ⁻¹ , with an intensity cutoff of 10 ⁻²⁶ cm molecule ⁻¹ , based on xMARVEL and the HotWat78 ¹²⁸ line positions	18
13. Room-temperature one-photon, dipole-allowed H ₂ ¹⁷ O linelist up to 30 000 cm ⁻¹ , with an intensity cutoff of 10 ⁻³⁰ cm molecule ⁻¹ , based on xMARVEL, HotWat78, ¹²⁸ and PE line positions	18
14. Room-temperature one-photon, dipole-allowed H ₂ ¹⁸ O linelist up to 30 000 cm ⁻¹ , with an intensity cutoff of 10 ⁻²⁶ cm molecule ⁻¹ , based on xMARVEL line positions	18
15. Room-temperature one-photon, dipole-allowed H ₂ ¹⁸ O linelist up to 30 000 cm ⁻¹ , with an intensity cutoff of 10 ⁻³⁰ cm molecule ⁻¹ , based on xMARVEL, HotWat78, ¹²⁸ and PE line positions	18

Theory” (Project No. 2004-035-1-100). This TG carefully considered the measured transitions of water vapor and validated and recommended a large number of them, as well as came up with corresponding empirical energy levels. The studies of the IUPAC TG addressed nine water isotopologues, H₂^XO,^{16–18} HD^XO,¹⁷ and D₂^XO¹⁹ ($X = 16, 17, 18$), and were based on the utilization of the MARVEL (Measured Active Rotational-Vibrational Energy Levels) technique,^{21–26} a global spectrum analysis tool under steady development.^{27–31} These datasets will be referred to as TG-H₂¹⁶O, TG-H₂¹⁷O, and TG-H₂¹⁸O in the remainder of this paper.

No major modifications of the IUPAC TG water data²⁰ have been made publicly available until 2020, when some of the authors of this study published³¹ an updated database, called W2020, of the parent water isotopologue, H₂¹⁶O. The present paper provides the second major extension of the IUPAC TG results, significantly

enlarging and upgrading the TG-H₂¹⁷O and TG-H₂¹⁸O datasets. This extension relies on the most recent developments related to the MARVEL code,^{29–31} resulting in what is called the xMARVEL³¹ protocol, and takes advantage of all the H₂¹⁷O and H₂¹⁸O transitions detected during the last decade^{32–66} as well as before that.^{67–127} After assembling the W2020 datasets and verifying their entries, it becomes feasible to consider how the new experimental high-resolution results can be utilized to further improve our knowledge on water spectroscopy and to present new recommendations for old energy levels, occasionally including modifications to their labels. Through the use of the xMARVEL technique, a considerable number of new, reliable empirical energy levels, with dependable uncertainties, are derived from the observed transitions.

Joint consideration of the W2020 lines and levels for the series H₂¹⁶O, H₂¹⁷O, and H₂¹⁸O allows improvements to be made to the individual datasets as well as the prediction of new lines for a number of applications. To realize these achievements, it was deemed necessary to slightly modify the W2020-H₂¹⁶O dataset³¹ as part of the present work. The smooth change in the rovibrational energies upon isotopic substitution facilitates the provision of a consistent set of quantum labels for this set of water isotopologues. The empirical results obtained can be employed to yield accurate estimates for yet unobserved transitions; thus, they provide highly useful input to future experimental studies of these water isotopologues. The experimental and empirical data present in the W2020 database should be sufficient to improve the result of atmospheric modeling efforts based on line-by-line information on water vapor. Extension of the empirical W2020 data to the visible region with accurate lines should facilitate such efforts. This extension can be achieved, for example, by the use of lines derived from pseudo-experimental (PE) levels.¹²⁸

The concept of PE levels was introduced recently by Polyansky *et al.*,¹²⁸ who showed that by combining the results of high-accuracy variational nuclear-motion calculations for one isotopologue of a molecule, say, H₂¹⁷O in our case, with empirical energy levels and variational results for a parent isotopologue, say, H₂¹⁶O, it becomes possible to predict the rovibrational levels of the daughter isotopologue with an accuracy as high as 0.01 cm⁻¹–0.02 cm⁻¹. A similar approach, albeit relying on perturbation theory rather than variational calculations, was proposed by Huang *et al.*¹²⁹ The procedure of Polyansky *et al.*¹²⁸ was used successfully by McKemmish *et al.*¹³⁰ to derive accurate line positions for minor isotopologues of the heavy diatomic molecule ⁴⁸Ti¹⁶O, contributing to the determination of Ti isotopic abundances in brown dwarfs based on high-resolution spectra.¹³¹ In order to complement the empirical energy levels deduced from the xMARVEL analyses for H₂¹⁷O and H₂¹⁸O, PE rovibrational energies are generated in this study for both minor water isotopologues. Carefully derived PE levels improve the coverage of water transitions up to and including the visible region.

The rest of this paper is organized as follows. In Sec. 2, the methodologies employed during this work are presented and the corresponding data-messaging treatments are sketched. Section 3 provides details about the construction of the W2020 datasets of the H₂¹⁶O, H₂¹⁷O, and H₂¹⁸O water isotopologues. Section 4 discusses the vibrational band origins (VBOs) covered by the W2020-H₂¹⁷O and W2020-H₂¹⁸O datasets. Section 5 describes how the validation of the transitions and especially of the empirical rovibrational energy levels of H₂¹⁷O and H₂¹⁸O was achieved. Section 6 presents the PE levels derived, as part of this

study, for both H₂¹⁷O and H₂¹⁸O, expanding the coverage of the empirical energy-level lists. A comparison of the W2020 data with entries of the HITRAN2016 information system is given in Sec. 7. Section 8 discusses the accuracy of recently measured quadruple-allowed transitions in light of the complete spectroscopic network (SN) of H₂¹⁶O.²⁴ As one stunning exercise of many similar possible ones, Sec. 9 reassesses the precision Lamb-dip spectroscopy data of one source, 10GaFaCaMa.³² Section 10 considers how the W2020 data presented may help atmospheric simulations. The paper ends with Sec. 11, where interesting and important conclusions are drawn as a summary of the present study.

2. Methods and Data Treatment

2.1. Spectroscopic networks

To provide the best estimates for the empirical rovibrational energies of H₂¹⁶O, H₂¹⁷O, and H₂¹⁸O, all of the (mainly experimental) rovibrational lines, collated from the literature, were processed in a simultaneous way by including them in SNs.^{22,24,28,30} SNs are formed by nodes (energy levels) connected by edges (measured or computed lines); the latter are directed from their lower energy levels to the upper ones, regardless of whether they were observed in absorption, in emission, or through techniques of action spectroscopy. Often, there are multiple measurements of the same transition; these correspond to multiple edges in the SN. A special characteristic of SNs is that the nodes define a potential function.

SNs often contain several components, that is, sets of energy levels not linked by any transition. If a component of the SN contains the lowest-energy state of a nuclear-spin isomer of the molecule considered, this component is referred to as a principal component (PC); otherwise, it is called a floating component (FC). Excluded energy levels,³⁰ whose determining transitions have all been removed for one reason or another, form special (single-node) FCs of the SN. For H₂¹⁶O, H₂¹⁷O, and H₂¹⁸O, transitions connecting states of their two nuclear-spin isomers (*ortho* and *para*) have not been detected;¹³² thus, the energy separation of the *ortho* and *para* PCs is not known from experiments. For further details about definitions and related notations concerning SNs and networks in general, see Sec. 2.1 of Ref. 30 and Ref. 133, respectively.

2.2. The xMARVEL procedure

MARVEL started out^{21–26} as a protocol for inverting, in a weighted linear-least-squares sense, line positions taken from (ultra)high-resolution laboratory spectra to the best (optimal) set of consistent rovibrational (occasionally rovibronic) energy levels. The original MARVEL protocol is built heavily on spectroscopic data management schemes advanced by Flaud *et al.*¹³⁴ and Tashkun *et al.*¹³⁵ (note that probably one of the very first such line inversion studies was published by Aslund¹³⁶). Over the years, there have been many developments^{27–31} improving how MARVEL treats and exploits experimental data. The different flavors of the MARVEL technique, including xMARVEL introduced in Refs. 30 and 31, have been used to treat nine isotopologues of water,^{16–20} three of which are the subject of the present investigation, as well as the laboratory spectroscopic data of a number of diatomics,^{137–141} triatomics,^{142–145} tetratomics,^{146–148} and beyond.¹⁴⁹

The xMARVEL procedure^{30,31} has been used extensively during the present study to treat experimental rovibrational data of H₂¹⁶O, H₂¹⁷O, and H₂¹⁸O. The corresponding xMARVEL input and output data files are provided in the [supplementary material](#).

2.3. Notation

xMARVEL requires that the upper and lower states of each transition have unique labels with a set of quantum numbers and perhaps some other useful information (such as symmetry), characteristic of the rovibrational states considered. For water isotopologues, it is customary to identify their rovibrational states using approximate normal-mode (ν_1, ν_2, ν_3) and rigid-rotor (J, K_a, K_c) quantum numbers, often referred to as $(\nu_1 \nu_2 \nu_3)_{J, K_a, K_c}$. In this list, J is the total rotational angular momentum quantum number, while K_a and K_c correspond to the projection of the rotational angular momentum on the molecular a and c axes, respectively. For H_2^XO ($X = 16, 17, 18$), ν_1, ν_2 , and ν_3 are the number of vibrational quanta in the symmetric stretch, bend, and asymmetric stretch modes, respectively. Note that for symmetric water isotopologues, local-mode quantum numbers give a better representation of the physical nature of the higher-excited stretching states.¹⁵⁰ One can map the vibrational quantum numbers from normal to local mode and *vice versa*,¹⁵¹ so either scheme can be used without loss of generality. For this reason, we retain the more conventional normal-mode labels when constructing the W2020 datasets.

Checking the correctness of the labels of the lower and upper states of the lines requires the understanding of symmetry characteristics. The symmetry characteristics and selection rules related to the approximate quantum numbers of H_2^{16}O are listed in Ref. 20; the same set of rules applies to $\text{H}_2^{17/18}\text{O}$.

2.4. Pseudo-experimental rovibrational levels

In order to provide increased coverage of the accurately known rovibrational energy levels of H_2^{17}O and H_2^{18}O , and the related transitions, we decided to augment the W2020 dataset of these species with so-called PE¹²⁸ energy levels. To justify this decision, we note that the accuracy of the PE energy levels is significantly better than that of their first-principles (FP) counterparts, upon which they are partially based (see below). The idea of the construction of PE energies for a daughter isotopologue from the knowledge of experimental (empirical) as well as FP energy levels of a major isotopologue was reported in Ref. 128. This approach is based on the approximate equality of the observed minus calculated (obs – calc) residuals of energy levels with the same vibrational and rotational assignment among the different isotopologues. In particular, in the present case of the water molecule, the obs – calc residuals for the rovibrational levels of H_2^{16}O are very similar to those characterizing the related states of H_2^{17}O and H_2^{18}O .

To provide a formal definition for the PE states, let us consider the following trivial connection:

$$E_{\nu,r}^{\text{expt}}(X) = E_{\nu,r}^{\text{FP}}(X) + R_{\nu,r}(X), \quad (1)$$

where $E_{\nu,r}^{\text{expt}}(X)$ and $E_{\nu,r}^{\text{FP}}(X)$ are the experimental (more precisely, empirical) and the FP energies of H_2^XO ($X = 16, 17, 18$), $\nu = (\nu_1 \nu_2 \nu_3)$ and $r = J_{K_a, K_c}$ denote the vibrational and rotational labels of the investigated level, respectively, and $R_{\nu,r}(X) = E_{\nu,r}^{\text{expt}}(X) - E_{\nu,r}^{\text{FP}}(X)$ is the residual between the experimental and the FP energies. By employing the $R_{\nu,r}(X) \approx R_{\nu,r}(16)$ approximation for $X = 17$ and $X = 18$,

$$E_{\nu,r}^{\text{expt}}(X) \approx E_{\nu,r}^{\text{FP}}(X) + R_{\nu,r}(16) \equiv E_{\nu,r}^{\text{PE}}(X) \quad (2)$$

is obtained, where $E_{\nu,r}^{\text{PE}}(X)$ is the PE energy of the (ν, r) state. In order to approach the accuracy of the empirical energy values derived in the present study, Eq. (2) needs to be modified to the form

$$E_{\nu,r}^{\text{PE}}(X) = E_{\nu,r}^{\text{FP}}(X) + R_{\nu,r}(16) + \Delta R_0(X), \quad (3)$$

where

$$\Delta R_0(X) = \frac{1}{N} \sum_{i=1}^N [R_{\nu^{[i]}, r_0}(X) - R_{\nu^{[i]}, r_0}(16)], \quad (4)$$

N is the total number of $\nu^{[i]}$ vibrational states considered in Eq. (4), and $r_0 = 0_{0,0}$. Our preliminary calculations suggest that the simple $\Delta R_0(17)$ and $\Delta R_0(18)$ corrections (estimated to be 0.006 cm^{-1} and 0.012 cm^{-1} , respectively) could be determined not only empirically, as suggested by Eq. (4), but also from vibrational non-adiabatic corrections.

3. The W2020 Datasets

The W2020 database can be considered as a significant update to and an extension of the datasets assembled by the IUPAC TG^{16–19} mentioned in the Introduction. Thus, the initial databases of this study were the experimental line lists of TG- H_2^{17}O and TG- H_2^{18}O .¹⁷ As to H_2^{16}O , the W2020 dataset of Ref. 31 is enlarged here, the latter itself being a significant update of the TG- H_2^{16}O list.¹⁸

3.1. H_2^{16}O

Although the W2020 dataset for H_2^{16}O was published only recently,³¹ the dataset was further investigated as part of this study in order to improve our treatment of the data for H_2^{17}O and H_2^{18}O . In particular, the sources 01NaUblPo,¹⁰² 17CaMiVaRe,⁵³ and 20MiBeOdTr,⁶³ containing dipole-allowed transitions, were added to the W2020- H_2^{16}O dataset.³¹ The sources 01NaUblPo,¹⁰² 17CaMiVaRe,⁵³ and 20MiBeOdTr⁶³ contain 1393, 183, and 604 assigned transitions, respectively, and what is especially important, inclusion of the transitions of 01NaUblPo¹⁰² yields 71 new empirical energy levels for H_2^{16}O . Due to the high quality of the assigned transitions in these three sources,^{53,63,102} it proved to be straightforward to expand the xMARVEL input with these new entries without any relabeling or significant uncertainty adjustments. Furthermore, in 2020, two studies reporting weak, quadrupole-allowed transitions^{152,153} of H_2^{16}O appeared, containing 21 lines. In Ref. 31, only the data of Ref. 152 were considered, while all the quadrupole data form part of our extended W2020- H_2^{16}O database. As a result of these changes, the original³¹/augmented W2020- H_2^{16}O datasets contain 270 745/286 987 non-redundant rovibrational transitions with 19 204/19 225 empirical energy levels. The updated and enlarged W2020- H_2^{16}O dataset can be found in the [supplementary material](#).

To facilitate the construction and improve the consistent labeling of the W2020- H_2^{17}O and W2020- H_2^{18}O databases, the original W2020- H_2^{16}O dataset was compared to the 20MiKaMoCa⁶⁶ linelist as this list contains entries for H_2^{17}O and H_2^{18}O as well. This comparison yielded a number of important observations worth detailing here. To aid understanding of what follows, a few details about the 20MiKaMoCa⁶⁶ linelist must be provided. Namely, the upper-state energies of the 20MiKaMoCa⁶⁶ linelist were derived either from ground-state combination-difference (CD) relations or from published theoretical energy-level lists, while the lower-state energies

were simply taken from TG-H₂¹⁶O. The CDs also utilized the TG-H₂¹⁶O lower-state energies when they were added to the wavenumbers extracted from intracavity laser absorption spectroscopy (ICLAS), Fourier-transform spectroscopy (FTS), cavity-ringdown spectroscopy (CRDS), comb-assisted CRDS (CA-CRDS), and Lamb-dip transitions.

Due to their significantly lower accuracy, all the 20MiKaMoCa⁶⁶ transitions based on theoretical predictions or ICLAS measurements were neglected during the present analysis. After the comparison of the original W2020-H₂¹⁶O database to the 20MiKaMoCa⁶⁶ lines, it was found that MARVEL reproduces 63 of the 77 Lamb-dip lines within $1 \times 10^{-4} \text{ cm}^{-1}$, 10 571 of the 11 775 CA-CRDS line positions within $1 \times 10^{-3} \text{ cm}^{-1}$, and 7427 of the 7607 CRDS/FTS lines within $1 \times 10^{-2} \text{ cm}^{-1}$. Although the 20MiKaMoCa lines are by and large in good agreement with their W2020 counterparts, some outliers, attributed to (at least) the following four factors, were revealed. First, compared to the TG-H₂¹⁶O database,¹⁸ the energy values of the W2020 dataset changed by a small but significant extent, on the order of 10^{-4} cm^{-1} – 10^{-3} cm^{-1} , even within the ground vibrational state. If the 20MiKaMoCa database was reconstructed using the significantly more reliable W2020 entries instead of their TG counterparts, much better agreement between the 20MiKaMoCa and W2020 linelists could be achieved. Second, there were several cases where, instead of utilizing the lone (non-confirmed) CA-CRDS or CRDS/FTS transitions, the upper-state W2020 energies were close to values suggested by a handful of emission lines, confirming each other in the corresponding CD relations. After increasing the uncertainties of these emission transitions, xMARVEL was able to reproduce this subset of 20MiKaMoCa⁶⁶ entries significantly better. Third, in a number of cases when the deviation between a xMARVEL and a 20MiKaMoCa line is larger than 0.01 cm^{-1} , the empirical (xMARVEL) energies are determined solely by emission measurements. In other words, we could not find the sources of certain CRDS/FTS lines reported in 20MiKaMoCa.⁶⁶ Without experimental information, nothing can be done within xMARVEL to improve this collection of empirical energies. Fourth, when two transitions have highly similar estimated accuracies, no individual uncertainties were reported for them in their literature sources, and the two transitions suggest two significantly different energies for the same state, the empirical energy of this state will be approximately the average of these different values with an appropriately increased uncertainty. This means that xMARVEL reproduces neither line perfectly, leading to considerable deviations from some of the 20MiKaMoCa predictions. This problem can be remedied once the experimental papers start reporting at least the correct order of magnitude of the individual uncertainties (e.g., 10^{-5} cm^{-1} , 10^{-4} cm^{-1} , 10^{-3} cm^{-1}) for all the reported transitions. Based on all these observations, we decided to update the W2020-H₂¹⁶O dataset of Ref. 31, both by making the necessary adjustments indicated by comparisons with the 20MiKaMoCa⁶⁶ linelist and by the availability of new sources.^{53,63,102,152,153} As is clear from Fig. 1, the updated W2020-H₂¹⁶O dataset is able to reproduce 10 939 CA-CRDS line positions (out of 11 775) and 7559 CRDS/FTS lines (out of 7607) within the above criteria, validating both linelists.

As a next important step, the empirical W2020-H₂¹⁶O line positions derived during this study from the enlarged and updated dataset were compared to those of the lines of the SISAM database.¹⁵⁴ The SISAM dataset contains 17 472 H₂¹⁶O lines in the range of 500.035 cm^{-1} – 7973.082 cm^{-1} . All SISAM lines could be nicely

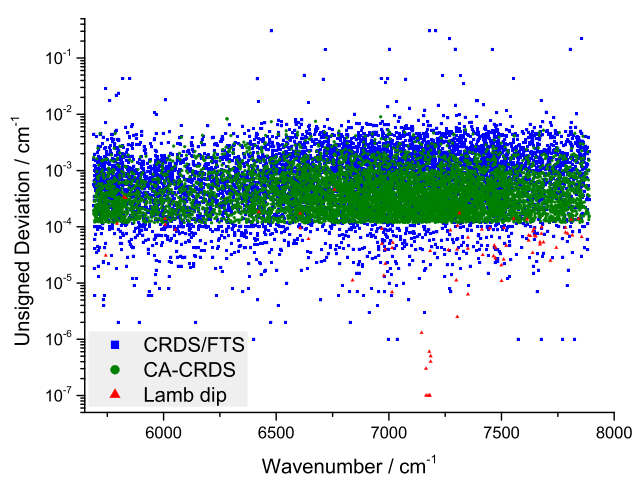


FIG. 1. Unsigned deviations of the 20MiKaMoCa⁶⁶ lines from their W2020-H₂¹⁶O counterparts.

matched with their W2020-H₂¹⁶O counterparts. In the 76 cases where probable labeling conflicts were found, due to the use of modified labels of the latest H₂¹⁶O publications included in W2020, they were excluded from the analysis. The list of the outlying SISAM lines can be found in the [supplementary material](#).

As clearly shown in Fig. 2, the agreement is excellent between the SISAM dataset and the new version of the W2020-H₂¹⁶O database. Overall, 15 821 SISAM lines can be reproduced within $5 \times 10^{-4} \text{ cm}^{-1}$. It is also important to point out that *all* the lines in SISAM with absorption intensities larger than $1 \times 10^{-26} \text{ cm molecule}^{-1}$ have corresponding counterparts in the updated W2020-H₂¹⁶O dataset. This means that if the W2020-H₂¹⁶O entries of this study are used in building a future H₂¹⁶O linelist, then there appears to be no need to employ the transition wavenumbers present in SISAM.

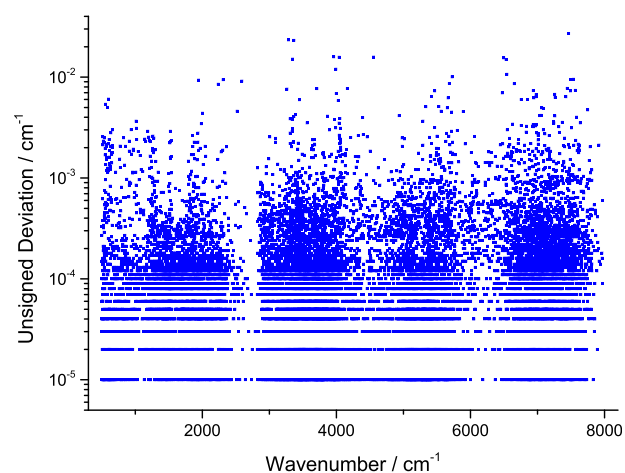


FIG. 2. Unsigned deviations of the SISAM¹⁵⁴ lines from their updated W2020-H₂¹⁶O counterparts.

3.2. H₂¹⁷O and H₂¹⁸O

The W2020-H₂¹⁷O and W2020-H₂¹⁸O datasets were assembled based on the following five major tasks: (a) construct the most complete catalog of published experimental lines; (b) set the best possible (often unreported) initial uncertainties of the observed line positions to help the uncertainty refinement process; (c) certify the existence of the empirical energy levels by comparison with their FP (in the present case HotWat78¹²⁸) counterparts; (d) create the best possible, consistent labels for the rovibrational states of the H₂^XO isotopologues, with $X = 16, 17,$ and 18 ; and (e) expand the transition database with certain unmeasured, unreported, or even artificial transitions, inspired by well-founded spectroscopic information,^{155,156} and derive further empirical energy levels for these minor water isotopologues.

As to task (a), we added 35 and 37 new sources to the TG-H₂¹⁷O and TG-H₂¹⁸O databases, respectively.¹⁷ Note that most of the new sources appeared after the compilation of Ref. 17, though some of them had just been omitted accidentally during collection of experimental spectroscopic data performed more than a decade ago. As a result, the W2020-H₂¹⁷O database contains 65 sources of experimental data (divided into 76 segments), while the W2020-H₂¹⁸O database is built up from 87 sources (distributed into 99 segments).

During task (b), we tried to find the best possible initial uncertainties, called estimated segment uncertainties (ESUs), for segments of the measured line positions. First, we tried to use directly the uncertainties given in the sources. If individual uncertainties were not available in the source (this is more the rule than the exception), the median of the refined transition uncertainties within a given segment was calculated. If this value, called median segment uncertainty (MSU), is close to ESU, then the ESU value was accepted; otherwise, it was replaced with MSU. In contrast to the W2020-H₂¹⁶O database, the H₂¹⁷O and H₂¹⁸O databases include only a few sources where their typical uncertainties had to be modified, compared to the values established for TG-H₂¹⁷O and TG-H₂¹⁸O.¹⁷ For example, the ESU of 99CaFlMaBy⁹⁹ was decreased from $1 \times 10^{-3} \text{ cm}^{-1}$ to $5 \times 10^{-4} \text{ cm}^{-1}$ for H₂¹⁷O and that of 05Tothb¹¹³ was decreased from $1 \times 10^{-3} \text{ cm}^{-1}$ to $5 \times 10^{-4} \text{ cm}^{-1}$ for H₂¹⁸O.

Relying on the complete experimental linelist with the best possible initial uncertainties, one can determine dependable empirical rovibrational energies *via* executing the latest version of the xMARVEL protocol.³¹ After the determination of the empirical energies, as part of task (c), one needs to check whether these energies have counterparts in the FP energy list (HotWat78),¹²⁸ within a tolerance of $10^{-4} \times E$ (where E is the energy of the xMARVEL state examined) inside a given (J , symmetry) block with the natural restriction that each FP state should be utilized only once. The transitions of those empirical states that could not be matched within this criterion were excluded from the database.

While performing task (d), we attempted to find the best possible set of consistent labels for each rovibrational state. As is well known,^{31,157-159} there are no theoretical techniques yielding unambiguous labels for high-lying vibrational bands; thus, sometimes, it is very hard to find the best labeling scheme for the rovibrational states. During the first phase of the present study, the labels of the W2020-H₂¹⁶O database³¹ were utilized as a guide to create consistent labels for the rovibrational states of H₂¹⁷O and H₂¹⁸O. It is expected that the differences among the rovibrational energy levels of H₂¹⁶O and H₂^XO ($X = 17$ or 18) with the same labels follow, as a function of K_a , a simple trend within a given vibrational band. If the difference deviates significantly from a well-established trendline, we

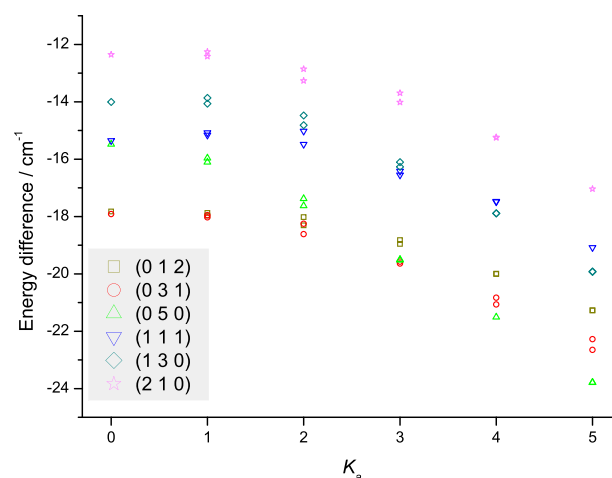


FIG. 3. Differences between the H₂¹⁶O and H₂¹⁸O rovibrational energies for the vibrational bands of the $P = 5$ polyad at $J = 5$.

decided to relabel that particular state of H₂^XO. To illustrate this simple procedure, the differences of some H₂¹⁶O and H₂¹⁸O energy levels are plotted in Fig. 3 as a function of K_a at fixed $J = 5$ and $P = 5$, where $P = 2\nu_1 + \nu_2 + 2\nu_3$ is the so-called polyad number. For high J values, say, those above $J = 15$, and higher vibrational excitations, there is not enough information to utilize such plots. Figure 3 shows that the differences decrease considerably faster in vibrational states with a high bending contribution compared to the stretching states. This is the reason why the bending trendline crosses that of the stretching one close to a particular K_a value (see Fig. 3). Unfortunately, near a crossing, the vibrational label becomes somewhat arbitrary. The correctness of the rovibrational labels is questioned when the calculated levels within the same symmetry block are closer to each other than 1 cm^{-1} . In these cases, the trendlines were used for verifying the labels. At the end, more than 200 and 400 rovibrational states were relabeled for H₂¹⁷O and H₂¹⁸O, respectively. Compared to the overall number of empirical energy levels known for these two minor water isotopologues, these changes are not drastic but significant for a number of applications, such as seeking PE energy levels (*vide infra*) or estimating pressure-broadening parameters. As a result, we believe that, whenever possible, the labels of the rovibrational states within the W2020 database of H₂¹⁶O, H₂¹⁷O, and H₂¹⁸O are consistent with each other.

During task (e), several transitions that cannot be (or have not been) measured were introduced into the W2020 datasets. For example, the disconnected *ortho* and *para* states were linked by so-called *magic numbers*, which correspond to the energy difference of the $(0\ 0\ 0)1_{0,1}$ and $(0\ 0\ 0)0_{0,0}$ states. In the case of H₂¹⁷O, the value⁹³ of $23.773\ 51(2) \text{ cm}^{-1}$ is adopted as the magic number, while for H₂¹⁸O, the value⁹³ of $23.754\ 902(5) \text{ cm}^{-1}$ is employed. Nearby *ortho* and *para* states (as confirmed by accurate FP calculations) were searched for in the FP databases.¹²⁸ Using these nearly degenerate states, *virtual lines* were introduced in order to maximize the number of empirically known energy levels for both H₂¹⁷O and H₂¹⁸O. 154 and 226 such virtual lines, collected into a source “20virt” and distributed in segments having different accuracy, are used for H₂¹⁷O and H₂¹⁸O, respectively. If the HotWat78 energy-level set indicated that the complementary (usually *para*) transition (separated by no more than

TABLE 1. Data source segments and their characteristics for the H₂¹⁷O molecule^a

Segment tag	Range	A/N/V	ESU	MSU	LSU	Recalib. factor
09PuCaHaVa ¹²⁷	6.471 2–18.413	5/5/5	2.00 × 10 ⁻⁸	2.00 × 10 ⁻⁸	3.00 × 10 ⁻⁸	
10GaFaCaMa ³²	7 084.0–7 222.3	2/2/2	3.34 × 10 ⁻⁷	3.34 × 10 ⁻⁷	3.34 × 10 ⁻⁷	
99MaNaNaOd ¹⁰⁰	15.671–177.15	125/125/125	1.40 × 10 ⁻⁶	1.53 × 10 ⁻⁶	2.72 × 10 ⁻⁵	
11Koshelev ³⁵	24.966–24.966	1/1/1	2.17 × 10 ⁻⁶	2.17 × 10 ⁻⁶	2.17 × 10 ⁻⁶	
71StBe ⁷⁰	0.451 50–6.471 2	2/2/2	3.34 × 10 ⁻⁶	3.34 × 10 ⁻⁶	3.34 × 10 ⁻⁶	
75LuHe ⁷⁴	18.413–24.966	2/2/2	3.34 × 10 ⁻⁶	9.97 × 10 ⁻⁶	1.51 × 10 ⁻⁵	
20virt	0.000 000–0.000 000	24/24/24	5.00 × 10 ⁻⁶	5.00 × 10 ⁻⁶	5.00 × 10 ⁻⁶	
20virt_S2	0.000 140–0.000 977	17/17/17	5.00 × 10 ⁻⁴	5.00 × 10 ⁻⁴	5.00 × 10 ⁻⁴	
20virt_S3	0.001 117–0.009 973	113/113/113	5.00 × 10 ⁻³	4.65 × 10 ⁻³	4.32 × 10 ⁻²	
92Toth ⁹³	23.774–23.774	1/1/1	2.00 × 10 ⁻⁵	2.00 × 10 ⁻⁵	2.00 × 10 ⁻⁵	
92Toth_S2 ⁹³	1 063.8–2 155.1	443/440/440	5.00 × 10 ⁻⁵	3.78 × 10 ⁻⁵	5.77 × 10 ⁻⁴	
92Toth_S3 ⁹³	1 011.9–2 224.2	258/258/255	5.00 × 10 ⁻⁴	1.86 × 10 ⁻⁴	3.22 × 10 ⁻³	
92Toth_S4 ⁹³	1 120.7–1 724.8	4/4/4	5.00 × 10 ⁻³	1.00 × 10 ⁻³	1.63 × 10 ⁻³	
93Toth ⁹⁴	1 314.1–3 938.9	84/84/84	5.00 × 10 ⁻⁵	5.00 × 10 ⁻⁵	4.39 × 10 ⁻⁴	
93Toth_S2 ⁹⁴	1 314.7–3 944.8	221/220/220	5.00 × 10 ⁻⁴	2.01 × 10 ⁻⁴	1.65 × 10 ⁻³	
93Toth_S3 ⁹⁴	1 898.6–3 679.7	33/33/33	5.00 × 10 ⁻³	1.03 × 10 ⁻³	5.59 × 10 ⁻³	
94Tothc ⁹⁵	3 254.1–4 080.4	350/350/350	5.00 × 10 ⁻⁵	4.96 × 10 ⁻⁵	7.44 × 10 ⁻⁴	
94Tothc_S2 ⁹⁵	3 223.7–4 242.7	407/406/406	5.00 × 10 ⁻⁴	2.59 × 10 ⁻⁴	2.21 × 10 ⁻³	
94Tothc_S3 ⁹⁵	3 223.2–4 216.0	68/68/68	5.00 × 10 ⁻³	1.35 × 10 ⁻³	3.14 × 10 ⁻²	
94Tothd ⁹⁶	6 752.6–7 301.0	11/11/11	5.00 × 10 ⁻⁵	5.00 × 10 ⁻⁵	2.60 × 10 ⁻⁴	
94Tothd_S2 ⁹⁶	6 619.9–7 639.2	580/579/578	5.00 × 10 ⁻⁴	4.21 × 10 ⁻⁴	3.76 × 10 ⁻²	
94Tothd_S3 ⁹⁶	6 616.8–7 540.1	264/263/261	5.00 × 10 ⁻³	1.29 × 10 ⁻³	3.01 × 10 ⁻²	
20MiBeOdTr ⁶³	48.030–665.56	619/618/618	5.00 × 10 ⁻⁵	4.32 × 10 ⁻⁵	6.69 × 10 ⁻³	
83Guelachv ⁸⁴	1 315.6–1 986.0	200/200/198	9.80 × 10 ⁻⁵	3.61 × 10 ⁻⁵	1.03 × 10 ⁻²	0.999 999 762 9
17CaMiVaRe ⁵³	4 249.9–4 533.7	20/19/19	1.00 × 10 ⁻⁴	1.00 × 10 ⁻⁴	5.78 × 10 ⁻³	
17MoMiKaBe ⁵⁵	7 443.3–7 921.0	1596/1595/1593	1.00 × 10 ⁻⁴	2.27 × 10 ⁻⁴	1.71 × 10 ⁻²	
18MiMoKaKa ⁵⁶	6 667.7–7 449.2	3544/3530/3528	1.00 × 10 ⁻⁴	2.61 × 10 ⁻⁴	1.48 × 10 ⁻²	
73CaFlGuAm ⁷³	3 581.5–3 909.4	58/58/56	5.00 × 10 ⁻⁴	4.50 × 10 ⁻⁴	4.97 × 10 ⁻³	
98Toth ⁹⁸	599.00–797.32	31/31/31	5.00 × 10 ⁻⁴	2.63 × 10 ⁻⁴	8.06 × 10 ⁻³	
99CaFlMaBy ⁹⁹	9 711.8–11 335	1063/1063/1062	5.00 × 10 ⁻⁴	5.00 × 10 ⁻⁴	1.37 × 10 ⁻²	
02MiTyStAl ¹⁰³	4 206.7–4 999.1	8/8/8	5.00 × 10 ⁻⁴	2.68 × 10 ⁻⁴	4.36 × 10 ⁻³	
05Tothb ¹¹³	5 018.3–5 684.7	312/312/312	5.00 × 10 ⁻⁴	2.15 × 10 ⁻⁴	4.19 × 10 ⁻³	
07JeDaReTy ¹²¹	4 206.7–6 599.5	574/567/563	5.00 × 10 ⁻⁴	5.59 × 10 ⁻⁴	2.47 × 10 ⁻²	
09LiNaKaCa ¹²⁶	5 907.8–6 725.2	212/211/211	5.00 × 10 ⁻⁴	6.54 × 10 ⁻⁴	1.71 × 10 ⁻²	
11LeNaCa ³⁶	13 541–14 107	391/391/388	5.00 × 10 ⁻⁴	1.00 × 10 ⁻³	3.46 × 10 ⁻²	
11LeNaCab ³⁷	12 585–13 555	126/125/124	5.00 × 10 ⁻⁴	5.00 × 10 ⁻⁴	2.54 × 10 ⁻²	
11MiKaWaCa ³⁸	7 408.2–7 902.2	346/344/341	5.00 × 10 ⁻⁴	6.07 × 10 ⁻⁴	4.14 × 10 ⁻²	
12LeMiMoKa ⁴⁰	6 886.9–7 404.9	696/672/669	5.00 × 10 ⁻⁴	4.53 × 10 ⁻⁴	1.34 × 10 ⁻²	
16MiLeKaMo ⁵¹	5 850.9–6 670.8	2512/2492/2487	5.00 × 10 ⁻⁴	4.89 × 10 ⁻⁴	3.64 × 10 ⁻²	
19MiKaVaMo ⁶⁰	5 693.5–5 988.4	188/185/185	5.00 × 10 ⁻⁴	3.79 × 10 ⁻⁴	4.11 × 10 ⁻²	
19MiMoKaKa ⁶¹	5 693.0–5 849.9	502/502/502	5.00 × 10 ⁻⁴	4.31 × 10 ⁻⁴	1.41 × 10 ⁻²	
19ReThReMi ⁶²	6 531.3–7 801.3	1136/1128/1128	5.00 × 10 ⁻⁴	7.32 × 10 ⁻⁴	1.82 × 10 ⁻²	
07MiLeKaCa ¹²³	5 988.1–7 015.5	236/235/234	6.00 × 10 ⁻⁴	8.15 × 10 ⁻⁴	2.27 × 10 ⁻²	
17LoBiWa ⁵⁴	1 853.7–3 988.3	620/620/620	6.00 × 10 ⁻⁴	1.52 × 10 ⁻⁴	4.95 × 10 ⁻³	
78KaKaKy ⁸⁰	100.37–301.14	20/20/19	1.00 × 10 ⁻³	1.13 × 10 ⁻³	1.48 × 10 ⁻²	
80KaKy ⁸²	53.510–727.83	371/371/371	1.00 × 10 ⁻³	1.00 × 10 ⁻³	3.34 × 10 ⁻²	
81Partridg ⁸³	16.081–46.917	17/17/17	1.00 × 10 ⁻³	1.02 × 10 ⁻³	3.01 × 10 ⁻³	
05TaNaBrTe ¹¹⁰	11 365–14 472	873/873/859	1.00 × 10 ⁻³	2.25 × 10 ⁻³	3.92 × 10 ⁻²	
08ToTe ¹²⁵	10 140–13 910	326/251/246	1.00 × 10 ⁻³	1.46 × 10 ⁻³	3.10 × 10 ⁻²	
12MiNaNiVa ⁴¹	6 691.3–8 883.6	130/128/128	1.00 × 10 ⁻³	1.89 × 10 ⁻³	1.60 × 10 ⁻²	
14ReOuMiWa ⁴⁷	6 619.2–9 187.3	616/584/583	1.00 × 10 ⁻³	1.22 × 10 ⁻³	3.32 × 10 ⁻²	
15CaMiLoKa ⁴⁸	7 915.6–8 332.8	232/229/229	1.00 × 10 ⁻³	1.00 × 10 ⁻³	3.28 × 10 ⁻²	

TABLE 1. (Continued.)

Segment tag	Range	A/N/V	ESU	MSU	LSU	Recalib. factor
18MiSeSi ⁵⁷	16 640–17 003	106/106/105	1.00×10^{-3}	5.17×10^{-3}	4.52×10^{-2}	
18TaMiWaLi ⁵⁸	12 278–12 893	1283/1280/1272	1.00×10^{-3}	1.24×10^{-3}	2.36×10^{-2}	
19LiLiZhWa ⁵⁹	12 057–12 260	441/437/424	1.00×10^{-3}	1.00×10^{-3}	2.17×10^{-2}	
20VaNaSeSi ⁶⁵	14 912–15 598	661/661/661	1.00×10^{-3}	1.67×10^{-3}	1.92×10^{-2}	
04MaRoMiNa ¹⁰⁸	6 170.8–6 746.9	232/231/228	2.00×10^{-3}	1.39×10^{-3}	3.82×10^{-2}	
13LeMiMoKa ⁴⁴	5 855.5–6 604.9	266/264/264	2.00×10^{-3}	1.18×10^{-3}	3.45×10^{-2}	
20SiSePoBy ⁶⁴	5 201.7–6 195.8	1071/1071/1070	2.00×10^{-3}	1.11×10^{-3}	4.05×10^{-2}	
20compl	176.60–15 436	66/66/64	2.00×10^{-3}	7.08×10^{-3}	3.80×10^{-2}	
05ToNaZoSh ¹¹¹	10 140–13 718	244/242/240	3.00×10^{-3}	4.26×10^{-3}	3.25×10^{-2}	
07MaToCa ¹²²	11 547–12 728	326/323/312	3.00×10^{-3}	2.82×10^{-3}	4.52×10^{-2}	
15MiSeSi ⁴⁹	15 127–15 941	106/106/106	3.00×10^{-3}	3.00×10^{-3}	2.03×10^{-2}	
69FrNaJo ⁶⁸	3 444.5–3 942.4	103/102/99	5.00×10^{-3}	4.97×10^{-3}	3.96×10^{-2}	
71WiNaJo ⁷¹	1 338.3–1 912.6	133/132/116	5.00×10^{-3}	6.87×10^{-3}	4.46×10^{-2}	
77ToFlCa ⁷⁶	5 174.2–5 524.9	84/81/78	5.00×10^{-3}	1.89×10^{-3}	4.50×10^{-2}	
77ToFlCab ⁷⁷	7 093.7–7 333.3	20/20/17	5.00×10^{-3}	7.23×10^{-3}	3.93×10^{-2}	
77Winther ⁷⁸	61.437–391.87	48/48/46	5.00×10^{-3}	7.83×10^{-3}	3.15×10^{-2}	
80CaFlPa ⁸¹	1 591.3–1 839.9	11/11/11	5.00×10^{-3}	2.29×10^{-3}	1.80×10^{-2}	
83PiCoCaFl ⁸⁵	3 648.9–3 830.1	2/2/2	5.00×10^{-3}	5.54×10^{-3}	9.70×10^{-3}	
05ToTe ¹¹²	7 424.1–9 051.8	178/178/175	5.00×10^{-3}	1.49×10^{-3}	2.94×10^{-2}	
06LiHuCaMa ¹¹⁷	8 563.1–9 331.9	466/466/465	5.00×10^{-3}	1.92×10^{-3}	3.04×10^{-2}	
06MaNaKaBy ¹¹⁹	12 406–12 641	12/12/12	5.00×10^{-3}	6.46×10^{-3}	1.72×10^{-2}	
06NaSnTaSh ¹²⁰	16 666–17 125	513/513/490	5.00×10^{-3}	5.00×10^{-3}	4.40×10^{-2}	
12VaMiSeSi ⁴³	13 545–13 923	81/78/78	5.00×10^{-3}	3.59×10^{-3}	2.36×10^{-2}	
78JoMc ⁷⁹	1 613.1–1 643.6	2/2/2	1.00×10^{-2}	2.78×10^{-2}	4.43×10^{-2}	

^aTags denote the segments used in this study. Bold entries are new segments compared to TG-H₂¹⁷O.¹⁷ The column “Range” indicates the range (in cm⁻¹) corresponding to validated wavenumbers within the transition list. A is the number of assigned transitions, N is the number of non-redundant lines (with distinct wavenumbers or labels), and V is the number of validated transitions obtained at the end of the xMARVEL analysis. In the heading of this table, ESU, MSU, and LSU denote the estimated, the median, and the largest segment uncertainties in cm⁻¹, respectively. Rows are arranged in the order of the ESUs with the restriction that the segments of the same data source should be listed consecutively.

5×10^{-3} cm⁻¹ based on FP information) is not reported in the data source of an experimental (mainly *ortho*) line with a σ wavenumber, then this complementary transition was added to the source “20compl” with the same σ wavenumber. Altogether, 66 and 319 complementary lines are included in the 20compl source for H₂¹⁷O and H₂¹⁸O, respectively. Finally, it is important to note that the W2020-H₂¹⁸O database contains calculated lines from the source 16CoCh.⁵⁰ This source was added to the W2020-H₂¹⁸O database because the accuracy of its records is comparable to that of the typical experimental uncertainty, allowing us to connect high-lying FCs to the PCs.

Tables 1 and 2 provide a summary of all the data sources treated during this work for H₂¹⁷O and H₂¹⁸O, respectively. These tables contain the wavenumber ranges and the number of assigned (A) and validated (V) transitions, as well as the number of non-redundant lines (N), with distinct tags for each segment. Tags set boldface in these tables signify the new sources, compared to Ref. 17, employed in the present study.

The W2020-H₂¹⁷O dataset is composed of 27 045 assigned and 26 819 non-redundant transitions (the latter having distinct wavenumbers or labels), a threefold increase when compared to the TG-H₂¹⁷O database,¹⁷ which contains only 9034 lines. As seen in Table 1, the source 18MiMoKaKa⁵⁶ reports the largest set of

experimentally determined lines (3530). The W2020 database of H₂¹⁸O lines and levels, comprising 66 166 assigned and 63 972 non-redundant transitions, became more than twice as large as the one in Ref. 17, which contained 31 730 lines.

The W2020-H₂¹⁷O database contains 5278 rovibrational energy levels related to the PCs, which means that there are twice as many energy levels in the W2020 database than in TG-H₂¹⁷O.¹⁷ In the case of W2020-H₂¹⁸O, the increase in the number of empirical energy levels is not nearly as significant: the W2020-H₂¹⁸O compilation provides 6865 rovibrational energy levels, while the TG-H₂¹⁸O dataset is built up from 5133.¹⁷ The empirical rovibrational energy levels of H₂¹⁷O and H₂¹⁸O form a complete set through 3204 cm⁻¹ and 4031 cm⁻¹, respectively. All the W2020-H₂¹⁷O and W2020-H₂¹⁸O empirical energy levels are presented in the [supplementary material](#).

4. Vibrational Band Origins

The VBOs defined by the W2020-H₂¹⁷O and W2020-H₂¹⁸O experimental line lists are displayed in Tables 3 and 4, respectively. The number of experimentally known VBOs is 37 and 52 for H₂¹⁷O and H₂¹⁸O, respectively (due to the smaller number of measurements, the number of known VBOs is considerably less than for H₂¹⁶O, where this number is 133). All the VBOs are below 17 000 cm⁻¹, and the

TABLE 2. Data source segments and their characteristics for the H₂¹⁸O molecule^a

Segment tag	Range	A/N/V	ESU	MSU	LSU	Recalib. factor
06GoMaGuKn ¹¹⁴	6.7849–18.269	6/6/6	1.33×10^{-7}	1.33×10^{-7}	5.00×10^{-7}	
11GaFaFaCa ³⁴	7 222.3–7 222.3	1/1/1	4.34×10^{-7}	4.34×10^{-7}	4.34×10^{-7}	
87BeKoPoTr ⁹¹	0.187 63–24.861	21/9/9	6.67×10^{-7}	6.67×10^{-7}	2.74×10^{-5}	
10GaFaCaMa ³²	7 084.0–7 241.6	18/18/18	1.00×10^{-6}	1.00×10^{-6}	1.03×10^{-6}	
99MaNaNaOd ¹⁰⁰	18.508–174.81	118/118/118	1.28×10^{-6}	1.40×10^{-6}	2.27×10^{-5}	
70PoJo ⁶⁹	0.187 63–0.187 63	1/1/1	3.34×10^{-6}	3.34×10^{-6}	3.34×10^{-6}	
71StBe ⁷⁰	0.187 63–6.784 9	2/2/2	3.34×10^{-6}	5.13×10^{-6}	6.93×10^{-6}	
72LuHeCoGob ⁷²	6.784 9–24.861	11/11/11	3.34×10^{-6}	3.34×10^{-6}	8.39×10^{-6}	
20virt	0.000 000–0.000 001	6/6/6	5.00×10^{-6}	5.00×10^{-6}	5.00×10^{-6}	
20virt_S2	0.000 016–0.000 093	10/10/10	5.00×10^{-5}	5.00×10^{-5}	5.00×10^{-5}	
20virt_S3	0.000 123–0.000 981	39/39/38	5.00×10^{-4}	5.00×10^{-4}	7.74×10^{-3}	
20virt_S4	0.001 028–0.009 990	171/171/171	5.00×10^{-3}	4.24×10^{-3}	4.78×10^{-2}	
92Toth ⁹³	23.755–23.755	1/1/1	1.00×10^{-5}	1.00×10^{-5}	1.00×10^{-5}	
92Toth_S2 ⁹³	1 061.7–2 219.2	503/503/500	5.00×10^{-5}	3.27×10^{-5}	7.11×10^{-4}	
92Toth_S3 ⁹³	1 009.6–2 198.8	247/247/245	5.00×10^{-4}	1.54×10^{-4}	1.17×10^{-2}	
92Toth_S4 ⁹³	1 055.9–2 192.4	29/29/29	5.00×10^{-3}	1.00×10^{-3}	1.06×10^{-3}	
93Toth ⁹⁴	1 341.9–3 874.1	186/186/186	5.00×10^{-5}	5.21×10^{-5}	8.54×10^{-4}	
93Toth_S2 ⁹⁴	1 312.2–3 879.5	265/265/262	5.00×10^{-4}	2.00×10^{-4}	1.55×10^{-2}	
93Toth_S3 ⁹⁴	2 969.9–3 622.9	10/10/10	5.00×10^{-3}	1.08×10^{-3}	4.80×10^{-3}	
94Tothc ⁹⁵	3 227.6–4 236.4	321/321/320	5.00×10^{-5}	4.64×10^{-5}	1.84×10^{-3}	
94Tothc_S2 ⁹⁵	3 117.1–4 290.8	590/589/582	5.00×10^{-4}	2.13×10^{-4}	8.13×10^{-3}	
94Tothc_S3 ⁹⁵	3 212.5–4 340.2	127/126/126	5.00×10^{-3}	1.00×10^{-3}	7.65×10^{-3}	
94Tothd ⁹⁶	7 114.4–7 360.1	22/22/22	5.00×10^{-5}	9.41×10^{-5}	4.44×10^{-4}	
94Tothd_S2 ⁹⁶	6 608.1–7 607.7	503/481/480	5.00×10^{-4}	3.29×10^{-4}	2.03×10^{-2}	
94Tothd_S3 ⁹⁶	6 608.0–7 639.3	440/430/426	5.00×10^{-3}	1.00×10^{-3}	4.82×10^{-2}	
06JoPaZeCo ¹¹⁵	1 483.9–1 485.0	2/2/2	5.00×10^{-5}	1.94×10^{-5}	2.88×10^{-5}	
17LoBiWa ⁵⁴	1 853.3–3 994.7	1036/1036/1036	5.00×10^{-5}	5.58×10^{-5}	6.24×10^{-3}	
20MiBeOdTr ⁶³	48.581–670.75	733/732/731	5.00×10^{-5}	4.34×10^{-5}	1.75×10^{-2}	
83Guelachv ⁸⁴	1 253.9–2 053.0	306/306/305	7.20×10^{-5}	3.08×10^{-5}	1.37×10^{-2}	0.999 999 773 1
17CaMiVaRe ⁵³	4 249.8–4 533.3	32/32/32	1.00×10^{-4}	5.72×10^{-4}	3.54×10^{-3}	
17MoMiKaBe ⁵⁵	7 443.8–7 919.0	639/637/636	1.00×10^{-4}	4.91×10^{-4}	1.94×10^{-2}	
18MiMoKaKa ⁵⁶	6 667.7–7 442.6	1840/1808/1808	1.00×10^{-4}	4.55×10^{-4}	1.66×10^{-2}	
85Johns ⁸⁸	33.179–280.32	145/145/145	2.00×10^{-4}	1.24×10^{-4}	1.05×10^{-2}	
73CaFlGuAm ⁷³	3 533.5–3 935.6	128/126/126	5.00×10^{-4}	2.65×10^{-4}	2.49×10^{-2}	
83PiCoCaFl ⁸⁵	3 512.4–3 889.6	35/33/33	5.00×10^{-4}	7.32×10^{-4}	2.43×10^{-3}	
83ToBr ⁸⁶	3 717.8–3 738.0	3/3/3	5.00×10^{-4}	1.68×10^{-4}	2.20×10^{-4}	
85ChMaFlCa ⁸⁷	4 433.7–6 086.9	1367/1363/1354	5.00×10^{-4}	2.66×10^{-4}	2.79×10^{-2}	
86ChMaCaFlb ⁸⁹	5 924.2–7 862.2	2137/2137/2118	5.00×10^{-4}	5.56×10^{-4}	2.88×10^{-2}	
86ChMaFlCa ⁹⁰	4 897.4–5 918.1	186/186/186	5.00×10^{-4}	4.33×10^{-4}	1.91×10^{-2}	
87ChMaFlCa ⁹²	9 639.6–11 374	2093/2093/2078	5.00×10^{-4}	4.59×10^{-4}	2.52×10^{-2}	
98Toth ⁹⁸	595.53–943.98	75/74/74	5.00×10^{-4}	1.92×10^{-4}	2.37×10^{-2}	
01MoSaGiCi ¹⁰¹	7 182.1–7 184.5	3/1/1	5.00×10^{-4}	1.31×10^{-4}	1.31×10^{-4}	
03MiTyMe ¹⁰⁶	399.30–806.26	167/151/151	5.00×10^{-4}	5.00×10^{-4}	3.04×10^{-2}	
06LiDuSoWa ¹¹⁶	1 082.9–5 997.3	5233/5025/4990	5.00×10^{-4}	3.74×10^{-4}	4.10×10^{-2}	
06LiNaSoVo ¹¹⁸	6 000.7–8 003.0	3168/3055/3050	5.00×10^{-4}	4.66×10^{-4}	4.60×10^{-2}	
07JeDaReTy ¹²¹	4 201.0–6 599.2	1054/967/967	5.00×10^{-4}	6.50×10^{-4}	3.65×10^{-2}	
08ToTe ¹²⁵	9 880.9–14 362	864/713/703	5.00×10^{-4}	3.58×10^{-4}	2.77×10^{-2}	
09LiNaKaCa ¹²⁶	5 905.8–6 725.3	2015/1959/1959	5.00×10^{-4}	5.00×10^{-4}	2.84×10^{-2}	
11MiKaWaCa ³⁸	7 410.5–7 917.1	537/512/508	5.00×10^{-4}	4.43×10^{-4}	4.13×10^{-2}	
12LeMiMoKa ⁴⁰	6 886.7–7 405.8	1014/880/880	5.00×10^{-4}	4.70×10^{-4}	1.05×10^{-2}	
12OuReMiTh ⁴²	1 005.7–2 331.9	1645/1508/1507	5.00×10^{-4}	2.43×10^{-4}	1.50×10^{-2}	
16MiLeKaMo ⁵¹	5 850.8–6 670.6	1170/999/999	5.00×10^{-4}	5.90×10^{-4}	2.32×10^{-2}	

TABLE 2. (Continued.)

Segment tag	Range	A/N/V	ESU	MSU	LSU	Recalib. factor
19MiKaVaMo ⁶⁰	5 693.0–5 990.5	204/200/200	5.00×10^{-4}	4.21×10^{-4}	2.55×10^{-2}	
19MiMoKaKa ⁶¹	5 693.0–5 848.8	178/177/177	5.00×10^{-4}	5.00×10^{-4}	2.32×10^{-2}	
07MiLeKaCa ¹²³	5 918.1–7 015.0	454/453/453	6.00×10^{-4}	7.35×10^{-4}	1.62×10^{-2}	
78KaKaKy ⁸⁰	55.233–370.51	62/61/60	1.00×10^{-3}	1.44×10^{-3}	1.56×10^{-2}	
80KaKy ⁸²	53.571–725.11	369/369/369	1.00×10^{-3}	1.00×10^{-3}	2.38×10^{-2}	
81Partridg ⁸³	21.588–46.800	16/14/14	1.00×10^{-3}	1.00×10^{-3}	2.36×10^{-3}	
95ByNaPeSc ⁹⁷	11 600–12 696	736/736/731	1.00×10^{-3}	1.56×10^{-3}	3.17×10^{-2}	
02MiTyStAl ¹⁰³	4 201.0–4 997.4	70/69/69	1.00×10^{-3}	1.29×10^{-3}	1.81×10^{-2}	
02ScLeCaBr ¹⁰⁴	13 485–14 384	42/42/28	1.00×10^{-3}	5.51×10^{-3}	2.71×10^{-2}	
05TaNaBrTe ¹¹⁰	12 405–14 518	1087/1078/1065	1.00×10^{-3}	1.69×10^{-3}	3.32×10^{-2}	
06MaNaKaBy ¹¹⁹	11 741–12 664	66/66/65	1.00×10^{-3}	3.36×10^{-3}	2.58×10^{-2}	
08NaVoMaTe ¹²⁴	12 209–12 607	4/4/3	1.00×10^{-3}	6.64×10^{-3}	1.14×10^{-2}	
11LeNaCa ³⁶	13 541–14 112	1788/1707/1699	1.00×10^{-3}	2.17×10^{-3}	3.09×10^{-2}	
11LeNaCab ³⁷	12 585–13 557	1214/1212/1203	1.00×10^{-3}	2.07×10^{-3}	3.95×10^{-2}	
12MiNaNiVa ⁴¹	6 522.5–9 136.7	1261/1170/1170	1.00×10^{-3}	1.10×10^{-3}	1.67×10^{-2}	
13MiSeSiVa ⁴⁵	15 002–15 779	466/466/465	1.00×10^{-3}	1.62×10^{-3}	4.71×10^{-2}	
14LiNaKaCa ⁴⁶	5 855.7–6 802.2	235/205/205	1.00×10^{-3}	1.08×10^{-3}	1.31×10^{-2}	
14ReOuMiWa ⁴⁷	6 519.2–9 222.4	1429/1343/1343	1.00×10^{-3}	1.35×10^{-3}	3.36×10^{-2}	
15CaMiLoKa ⁴⁸	7 917.1–8 337.1	425/412/412	1.00×10^{-3}	1.00×10^{-3}	4.15×10^{-2}	
16CoCh ⁵⁰	10.756–4 983.9	7385/7379/7353	1.00×10^{-3}	1.00×10^{-3}	4.31×10^{-2}	
18MiSeSi ⁵⁷	16 463–17 192	987/987/967	1.00×10^{-3}	2.45×10^{-3}	4.38×10^{-2}	
18TaMiWaLi ⁵⁸	12 278–12 794	411/389/389	1.00×10^{-3}	1.70×10^{-3}	2.52×10^{-2}	
19LiLiZhWa ⁵⁹	12 055–12 260	161/156/156	1.00×10^{-3}	2.03×10^{-3}	4.65×10^{-2}	
19ReThReMi ⁶²	6 527.0–8 010.9	4236/4191/4189	1.00×10^{-3}	1.00×10^{-3}	4.57×10^{-2}	
20VaNaSeSi ⁶⁵	15 057–15 495	94/92/90	1.00×10^{-3}	1.98×10^{-3}	1.82×10^{-2}	
03ToTeShZo ¹⁰⁷	9 980.8–12 517	580/580/574	2.00×10^{-3}	1.26×10^{-3}	3.62×10^{-2}	
04MaRoMiNa ¹⁰⁸	6 134.5–6 748.5	490/472/458	2.00×10^{-3}	1.40×10^{-3}	4.73×10^{-2}	
04TaSnUbTe ¹⁰⁹	16 577–17 121	375/375/312	2.00×10^{-3}	5.38×10^{-3}	4.85×10^{-2}	
13LeMiMoKa ⁴⁴	5 852.2–6 606.3	598/550/550	2.00×10^{-3}	1.03×10^{-3}	1.42×10^{-2}	
20compl	33.197–16 957	319/319/289	2.00×10^{-3}	4.95×10^{-3}	4.72×10^{-2}	
05ToNaZoSh ¹¹¹	9 251.5–14 384	736/729/724	3.00×10^{-3}	3.70×10^{-3}	4.16×10^{-2}	
07MaToCa ¹²²	11 520–12 810	1833/1693/1670	3.00×10^{-3}	2.33×10^{-3}	4.89×10^{-2}	
12DoTeOrCh ³⁹	6 508.3–6 959.8	343/343/343	3.00×10^{-3}	1.21×10^{-3}	1.61×10^{-2}	1.000 002 863 4
15MiSeSi ⁴⁹	15 002–16 014	816/444/444	3.00×10^{-3}	3.00×10^{-3}	4.72×10^{-2}	
69FrNaJo ⁶⁸	3 347.7–4 028.6	618/616/578	5.00×10^{-3}	6.38×10^{-3}	4.92×10^{-2}	
71WiNaJo ⁷¹	1 334.3–1 955.0	234/234/214	5.00×10^{-3}	5.26×10^{-3}	4.74×10^{-2}	
76FlGi ⁷⁵	13.030–39.995	11/11/11	5.00×10^{-3}	1.09×10^{-3}	4.46×10^{-3}	
77ToFlCa ⁷⁶	5 036.9–5 638.0	527/527/511	5.00×10^{-3}	2.56×10^{-3}	4.68×10^{-2}	
77ToFlCab ⁷⁷	6 974.6–7 386.8	372/372/351	5.00×10^{-3}	5.09×10^{-3}	4.63×10^{-2}	
77Winther ⁷⁸	54.496–524.06	122/122/117	5.00×10^{-3}	5.78×10^{-3}	4.89×10^{-2}	
02TaBrTe ¹⁰⁵	12 403–14 494	747/747/683	5.00×10^{-3}	1.36×10^{-3}	4.81×10^{-2}	
05ToTe ¹¹²	7 428.4–9 270.6	502/502/491	5.00×10^{-3}	1.20×10^{-3}	4.60×10^{-2}	
06LiHuCaMa ¹¹⁷	8 012.1–9 336.8	1533/1533/1532	5.00×10^{-3}	1.64×10^{-3}	3.74×10^{-2}	
11BeMiCa ³³	13 563–14 039	19/19/19	5.00×10^{-3}	7.30×10^{-3}	2.55×10^{-2}	
12VaMiSeSi ⁴³	13 397–14 442	724/709/707	5.00×10^{-3}	3.15×10^{-3}	3.37×10^{-2}	
69BePoTo ⁶⁷	178.18–397.46	10/10/8	1.00×10^{-2}	1.00×10^{-2}	2.31×10^{-2}	1.000 088 431 0
78JoMc ⁷⁹	1 640.2–1 693.7	2/2/2	1.00×10^{-2}	3.94×10^{-2}	4.57×10^{-2}	

^aTags denote the segments used in this study. Bold entries are new segments compared to TG-H₂¹⁸O. The column “Range” indicates the range (in cm⁻¹) corresponding to the validated wavenumbers within the transition list. A is the number of assigned transitions, N is the number of non-redundant lines (with distinct wavenumbers or labels), and V is the number of validated transitions obtained at the end of the xMARVEL analysis. In the heading of this table, ESU, MSU, and LSU denote the estimated, the median, and the largest segment uncertainties in cm⁻¹, respectively. Rows are arranged in the order of the ESUs with the restriction that the segments of the same data source should be listed consecutively.

TABLE 3. VBOs within the W2020-H₂¹⁷O dataset^a

($\nu_1 \nu_2 \nu_3$)	VBO/cm ⁻¹	($\nu_1 \nu_2 \nu_3$)	VBO/cm ⁻¹
(0 0 0)	0.0	(2 0 1)	10 598.475 61(50)
(0 1 0)	1591.325 696(61)	(1 0 2)	10 853.505 32(50)
(0 2 0)	3144.980 73(13)	(0 0 3)	11 011.882 91(50)
(1 0 0)	3653.142 265(50)	(1 3 1)	11 792.824 6(25)
(0 0 1)	3748.318 070(54)	(3 1 0)	12 122.203 6(10)
(1 1 0)	5227.705 62(50)	(2 1 1)	12 132.992 8(10)
(0 1 1)	5320.251 07(14)	(1 1 2)	12 389.097 8(10)
(0 4 0)	6121.547 92(50)	(0 1 3)	12 541.226 8(13)
(1 2 0)	6764.725 64(79)	(2 2 1)	13 631.501 51(50)
(0 2 1)	6857.272 54(10)	(3 0 1)	13 812.158 31(50)
(2 0 0)	7193.244 79(10)	(1 0 3)	14 296.277 5(20)
(1 0 1)	7238.713 84(17)	(0 7 1)	13 808.301 31(50)
(0 0 2)	7431.076 86(25)	(2 3 1)	15 095.165 8(10)
(1 3 0)	8260.775 60(50)	(4 1 0)	15 322.533 2(10)
(0 3 1)	8356.527 88(10)	(3 1 1)	15 325.615 5(12)
(2 1 0)	8749.903 61(10)	(1 1 3)	15 807.053 1(30)
(1 1 1)	8792.550 69(10)	(3 2 1)	16 797.164 2(34)
(0 1 2)	8982.869 2(50)	(4 0 1)	16 875.619 6(10)
(1 2 1)	10 311.202 51(50)		

^aThe label ($\nu_1 \nu_2 \nu_3$) denotes a specific VBO, where ν_1 , ν_2 , and ν_3 are the standard normal-mode quantum numbers describing the symmetric stretch, bend, and asymmetric stretch vibrational excitations, respectively. The uncertainties related to the last two digits of the VBOs are provided in parentheses.

highest ones [(3 2 1), (4 0 1), and (0 4 3)] belong to the $P = 10$ polyad for both isotopologues.

For H₂¹⁷O, already the (0 3 0) bending overtone, at about 4660 cm⁻¹, is missing. Similarly, the (0 5 0) bending overtone is not present among the $P = 5$ VBOs. The coverage becomes much less complete above 11 000

cm⁻¹, which is about the height of the barrier to linearity of water.^{160–162} For H₂¹⁸O, the situation is similar: the first missing VBO is the (0 5 0) bending overtone. Beyond $P = 5$, the high bending excitations are systematically missing. It would be of interest to design high-resolution spectroscopic experiments aiming at the determination of the missing VBOs of these two minor water isotopologues.

The accuracy of the VBOs appears to be outstanding for both H₂¹⁷O and H₂¹⁸O. Even the least accurately known fundamental of H₂¹⁷O, the (0 1 0) bending fundamental, has an uncertainty of 6.1×10^{-5} cm⁻¹. For H₂¹⁸O, the least accurate fundamental, (1 0 0), is derived with a remarkable uncertainty of 6.1×10^{-5} cm⁻¹.

5. Validation of the W2020 Database Entries

As an independent validation of the transition wavenumbers, the derived empirical rovibrational energies and the labels of the W2020-H₂¹⁷O and W2020-H₂¹⁸O datasets were compared in a systematic and mostly automated way with the results of variational nuclear-motion calculations¹²⁸ and the energies of the so-called SISAM database.¹⁵⁴ The SISAM dataset¹⁵⁴ was probably the largest and most accurate energy-level set for both H₂¹⁷O and H₂¹⁸O available prior to this study. These comparisons were executed in order to identify and exclude from the W2020 database those transitions that would lead to energy levels with large deviations from well-established FP or empirical/experimental values.

Figures 4 and 5 show the unsigned deviations (UDs) corresponding to the comparison of the W2020 and SISAM energy levels for H₂¹⁷O and H₂¹⁸O, respectively. As can be seen there, the average UD is about 5×10^{-4} cm⁻¹ for both molecules. These figures also reveal that occasionally the differences are quite large (UD > 0.1 cm⁻¹). These large deviations may be attributed to those energy values of the SISAM dataset that were deduced from only very few (one or two) observed (but unreported) transitions *via* CD relations. As an example,

TABLE 4. VBOs within the W2020-H₂¹⁸O dataset^a

($\nu_1 \nu_2 \nu_3$)	VBO (cm ⁻¹)	($\nu_1 \nu_2 \nu_3$)	VBO (cm ⁻¹)	($\nu_1 \nu_2 \nu_3$)	VBO (cm ⁻¹)
(0 0 0)	0.0	(0 1 2)	8 967.562 9(22)	(2 2 1)	13 612.710 7(10)
(0 1 0)	1588.275 697(20)	(0 4 1)	9 795.331 50(50)	(4 0 0)	13 793.260 7(10)
(0 2 0)	3139.050 022(14)	(2 2 0)	10 256.584 86(50)	(3 0 1)	13 795.401 00(50)
(1 0 0)	3649.685 347(61)	(1 2 1)	10 295.634 00(40)	(1 2 2)	13 870.485 5(10)
(0 0 1)	3741.566 834(52)	(0 2 2)	10 483.221 46(50)	(0 2 3)	14 015.510 7(10)
(0 3 0)	4648.477 21(15)	(3 0 0)	10 573.916 86(50)	(2 0 2)	14 187.987 4(50)
(1 1 0)	5221.243 96(50)	(2 0 1)	10 585.285 00(10)	(1 0 3)	14 276.337 8(10)
(0 1 1)	5310.462 005(51)	(1 0 2)	10 839.955 96(50)	(0 7 1)	13 784.246 1(10)
(0 4 0)	6110.423 71(15)	(0 0 3)	10 993.680 65(25)	(2 3 1)	15 073.955(20)
(1 2 0)	6755.510 76(20)	(2 3 0)	11 734.525 1(30)	(4 1 0)	15 303.032 1(10)
(0 2 1)	6844.598 59(10)	(1 3 1)	11 774.707 6(10)	(3 1 1)	15 305.804 6(10)
(2 0 0)	7185.877 68(10)	(0 3 2)	11 963.537 2(30)	(2 1 2)	15 703.506 2(30)
(1 0 1)	7228.877 76(10)	(3 1 0)	12 106.977 7(30)	(1 1 3)	15 784.299 0(14)
(0 0 2)	7418.723 44(68)	(2 1 1)	12 116.797 6(10)	(3 2 1)	16 775.383 7(28)
(1 3 0)	8249.038 37(50)	(1 1 2)	12 372.704 9(10)	(4 0 1)	16 854.990 9(20)
(0 3 1)	8341.104 45(10)	(0 1 3)	12 520.122 0(10)	(0 4 3)	16 906.206 5(10)
(2 1 0)	8739.528 6(28)	(2 4 0)	13 167.718 4(10)		
(1 1 1)	8779.718 98(21)	(1 4 1)	13 212.678 2(10)		

^aSee footnote a to Table 3.

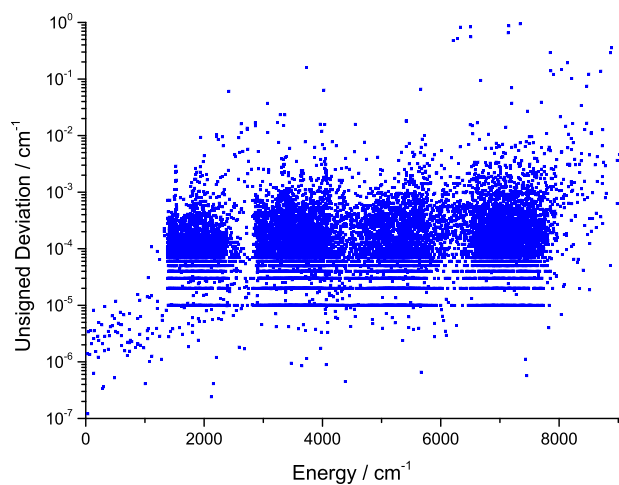


FIG. 4. Unsigned deviations of the SISAM¹⁵⁴ states from their W2020-H₂¹⁷O counterparts.

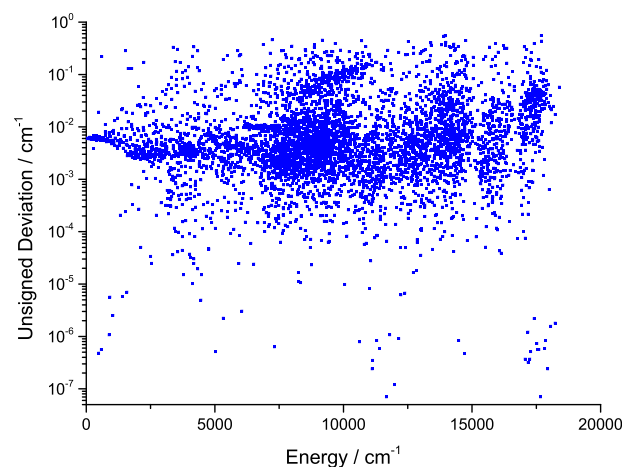


FIG. 6. Unsigned deviations of the HotWat78¹²⁸ energies from their W2020-H₂¹⁷O counterparts.

one of the largest deviations is for the H₂¹⁷O level (0 1 1)14_{1,14}, with an UD of 0.94 cm⁻¹. The W2020-H₂¹⁷O estimate, 7341.595 03(50) cm⁻¹, relies on two experimental lines, of 07JeDaReTy¹²¹ and 20SiSePoBy,⁶⁴ while the SISAM value, 7342.538 51(300) cm⁻¹, can be found in Table 2 of 05Tothb,¹¹³ and according to this table, it was calculated from one line not listed in 05Tothb. In addition, one can extract 7341.60 cm⁻¹ from the HotWat78 energy list, which corroborates the W2020 energy. Based on these findings, we feel that the SISAM datum should be incorrect, and, therefore, we decided to retain our estimate, confirmed by two independent data sources, in the W2020-H₂¹⁷O dataset. A detailed, one-by-one analysis of the outliers of Figs. 4 and 5 is beyond the scope of this paper. The list of the incorrect SISAM lines can be found in the [supplementary material](#).

The empirical energy levels of this study were also matched with their FP counterparts listed in the HotWat78¹²⁸ state list. The UDs for H₂¹⁷O and H₂¹⁸O are plotted in Figs. 6 and 7, respectively. Figures 6 and 7 show that for both molecules, the average UD is about 0.01 cm⁻¹, a very pleasing agreement from the point of view of the underlying fourth-age¹⁴ quantum-chemical computations. This means that the FP energy levels are of considerable accuracy, significantly better than what could have been achieved even just a decade ago, mostly due to our improved understanding of how potential energy hypersurfaces can be refined based on available empirical energy values. Thus, the line positions calculated from FP energies and augmented with high-accuracy FP intensities are of considerable utility for the design of new experiments aimed at the observation of experimentally unknown rovibrational states.

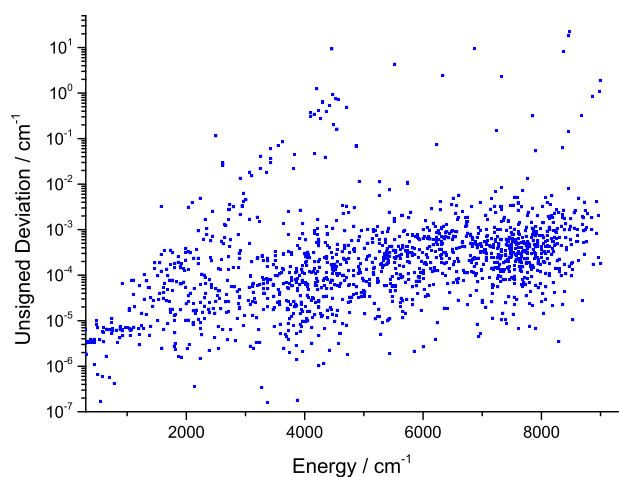


FIG. 5. Unsigned deviations of the SISAM¹⁵⁴ states from their W2020-H₂¹⁸O counterparts.

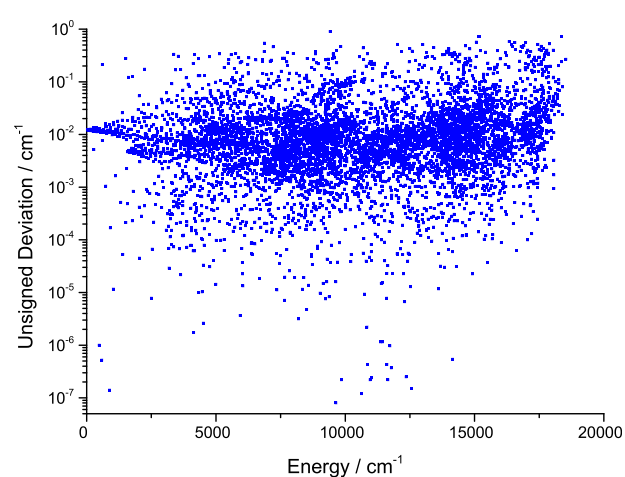


FIG. 7. Unsigned deviations of the HotWat78¹²⁸ energies from their W2020-H₂¹⁸O counterparts.

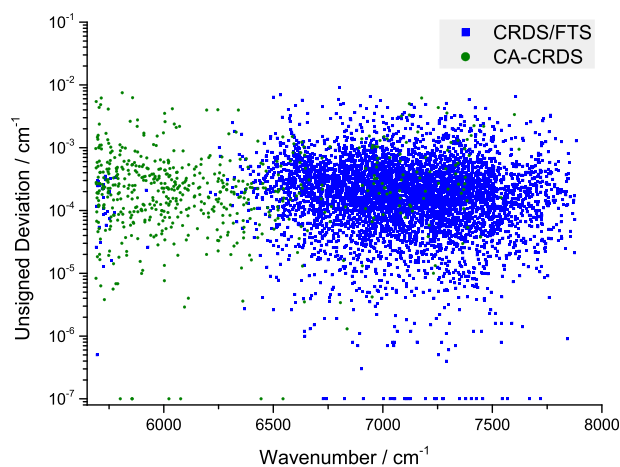


FIG. 8. Unsigned deviations of the 20MiKaMoCa⁶⁶ lines from their W2020-H₂¹⁷O counterparts.

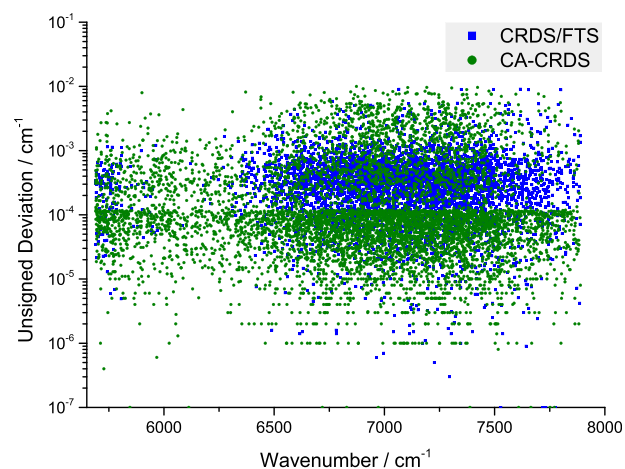


FIG. 9. Unsigned deviations of the 20MiKaMoCa⁶⁶ lines from their W2020-H₂¹⁸O counterparts.

Our H₂¹⁷O and H₂¹⁸O xMARVEL line lists were also compared with the 20MiKaMoCa⁶⁶ lines (see Figs. 8 and 9, respectively). Figure 8 shows that all H₂¹⁷O CRDS/FTS lines could be reproduced within 8×10^{-3} cm⁻¹. In the case of the H₂¹⁷O CA-CRDS lines, 4399 lines out of 5329 could be reproduced within 5×10^{-4} cm⁻¹, and only 74 labeling conflicts were found. As to H₂¹⁸O, 43 and 83 discrepancies were identified between the 20MiKaMoCa and W2020 labels for the CA-CRDS and CRDS/FTS lines, respectively. Figure 9 shows that for H₂¹⁸O, all the CRDS/FTS lines could be reproduced within 9×10^{-3} cm⁻¹ and 3367 out of 4570 CA-CRDS lines could be matched within 5×10^{-5} cm⁻¹.

6. Pseudo-experimental Rovibrational Levels

In Sec. 2.4, a procedure was described for obtaining PE energy levels for H₂¹⁷O and H₂¹⁸O with an accuracy approaching that of Fourier-transform infrared (FT-IR) measurements, based on the available empirical and FP energies of H₂¹⁶O. The first set of PE levels for H₂¹⁷O and H₂¹⁸O, relying on empirical energy values for H₂¹⁶O available at that time, was reported in Ref. 128. When these levels were tested against empirical levels of H₂¹⁶O of this study, it turned out that only about 95% of the PE levels were within the standard deviation of 0.02 cm⁻¹. The outliers helped us to derive criteria, detailed below, to remove insufficiently accurate PE levels, yielding the final set reported in this study. For cleansing the PE energy-level set, we adopted what we call the F and G criteria.

Criterion F is based on the quantity

$$F_{v,r} = 2E_{v,r}^{\text{PE}}(17) - E_{v,r}^{\text{PE}}(16) - E_{v,r}^{\text{PE}}(18), \quad (5)$$

reflecting the empirical connection

$$E_{v,r}^{\text{PE}}(17) \approx [E_{v,r}^{\text{PE}}(16) + E_{v,r}^{\text{PE}}(18)]/2. \quad (6)$$

Through the analysis of the $F_{v,r}$ residuals, one can monitor the smoothness of the changes within the H₂¹⁶O–H₂¹⁷O–H₂¹⁸O series. If the $F_{v,r}$ values are in the $[F_{\min}, F_{\max}]$ interval, where F_{\min} and F_{\max} are selected to be 0 cm⁻¹ and 7 cm⁻¹, respectively, and the related K_a dependence is adequately smooth, then we say that the underlying PE levels satisfy criterion F. In the opposite case, the anomalous PE levels,

not following a rigorous trend, have been excluded from further consideration.

Criterion G involves the use of the residuals

$$G_{v,r}(X) = E_{v,r}^{\text{PE}}(X) - E_{v,r}^{\text{ref}}(X), \quad (7)$$

where $E_{v,r}^{\text{ref}}(X)$ ($X = 17, 18$) denotes the accurate reference energy values taken from 08ShZoOvPo.¹⁶³ If $G_{v,r}(X) \in [G_{\min}, G_{\max}]$ for a given (v, r) state, where G_{\min} and G_{\max} are set to -0.07 and $+0.07$ cm⁻¹, respectively, then it is said that the underlying PE level obeys criterion G. Otherwise, this PE state is deemed to be unreliable.

The parameters of the F and G criteria, that is, F_{\min} , F_{\max} , G_{\min} , and G_{\max} , were chosen so that about 99% of the newly derived levels of Refs. 55, 57, and 58 coincided with our PE levels within 0.0045 cm⁻¹ for H₂¹⁷O and 0.0090 cm⁻¹ for H₂¹⁸O. The PE levels obtained were then compared with the much more extensive xMARVEL states of this study. This comparison also helped to deduce a consistent set of labels for the H₂¹⁶O–H₂¹⁷O–H₂¹⁸O series.

In particular, from the about 19 200 H₂¹⁶O levels of this study, about 14 950 and 14 650 PE energy levels were obtained for H₂¹⁷O and H₂¹⁸O, respectively, without the use of the F and G criteria. The loss of more than 4000 levels is due to issues with the unique identification of the FP states beyond the W2020 list. The joint use of the F and G criteria reduces the number of PE levels to 10 600 and 10 060 for H₂¹⁷O and H₂¹⁸O, respectively. These constitute the final PE energy collections of this study, which have average absolute deviations of 0.004 cm⁻¹ and 0.008 cm⁻¹ against the W2020-H₂¹⁷O and W2020-H₂¹⁸O datasets, respectively. Ignoring those states whose empirical energies are available in the W2020-H₂^XO datasets, 9925/6270 and 8409/4602 PE levels were obtained for H₂¹⁷O and H₂¹⁸O, respectively, without/with the use of the F and G criteria. These four datasets are reported in the [supplementary material](#). Table 5 shows statistics related to the comparison of the PE energies with their xMARVEL counterparts.

7. Comparison with HITRAN2016

The HITRAN2016 information system⁴ embraces a considerable number of transitions for H₂¹⁷O and H₂¹⁸O, as they are needed in a number of engineering and scientific applications, including

TABLE 5. Comparison of the PE energies with their xMARVEL counterparts

Absolute residual (cm ⁻¹)	H ₂ ¹⁷ O	H ₂ ¹⁸ O	Comment
<0.005	2777	2025	Perfect
0.005–0.05	1475	3288	Good
>0.05	61	105	Inaccurate
All	4313	5428	

atmospheric modeling (see Sec. 10, as well). For H₂¹⁷O, there are 27 543 transitions going up to 19 945.257 cm⁻¹, while for H₂¹⁸O 39 901 transitions can be found in HITRAN2016, covering the range of 0.052 cm⁻¹–19 917.617 cm⁻¹. Since xMARVEL works with the measured line positions and the labels of the experimental transitions and it results in empirical energy levels, only three types of spectroscopic information, i.e., the lower state energy values, the transition wavenumbers, and their assignments, were examined within HITRAN2016. After a detailed comparison of the W2020-H₂¹⁷O and W2020-H₂¹⁸O databases with their HITRAN2016 analogs, issues falling into three main categories could be diagnosed.

- I. **Forbidden transitions.** Employing the rovibrational symmetry of the lower and upper states, 159 and 10 forbidden transitions were discovered in HITRAN2016 for H₂¹⁷O and H₂¹⁸O, respectively. There is no such trouble with the W2020 datasets. The problems observed are collated in the [supplementary material](#). The cause of these incorrect lines is not completely clear, but these issues can be remedied straightforwardly during the construction of the next version of HITRAN.
- II. **Missing upper labels.** Both HITRAN2016 datasets exhibit a significant number of transitions, namely, 8258 (H₂¹⁷O) and 5588 (H₂¹⁸O), where the labels of the upper states are missing. For many of these unassigned upper states (697 and 402, respectively), feasible W2020 recommendations were found. The other unknown upper levels within HITRAN2016 are derived from theoretical computations¹⁶⁴ and not from measurements; thus, new experiments need to be performed to properly characterize the remaining unassigned lines. The list of the HITRAN2016 lines with missing labels and the corresponding W2020 recommendations is presented in the [supplementary material](#). Experimental high-resolution spectroscopists are encouraged to utilize this list, as well as the collection of the unlabeled transitions, to ensure an even more complete coverage of H₂¹⁷O and H₂¹⁸O spectra for future HITRAN editions. At the same time, it is important to point out that the intensities of the unassigned lines, where available, are quite low; therefore, these HITRAN entries may not be overly important for most applications where line-by-line databases of water isotopologues are needed.
- III. **Inaccurate line positions and labeling conflicts.** Matching HITRAN2016 lines with their xMARVEL-predicted counterparts was guided by the HITRAN2016 labels, adopting a reasonable matching condition,

$$|\sigma_{\text{HITRAN}} - \sigma_{\text{xMARVEL}}| \leq \max(10^{-6} \times E_{\text{HITRAN}}^{\text{up}}, \delta_{\text{xMARVEL}}), \quad (8)$$

where σ_{HITRAN} and σ_{xMARVEL} are the HITRAN and xMARVEL predictions of a particular line, respectively, $E_{\text{HITRAN}}^{\text{up}}$ is the upper energy of the given transition in HITRAN2016, and δ_{xMARVEL} is the

estimated uncertainty of σ_{xMARVEL} . In total, 949 and 1057 lines not satisfying Eq. (8) were found and explored for H₂¹⁷O and H₂¹⁸O, respectively. There are at least three feasible reasons that help explain the mismatches. First, some line positions are different due to a labeling conflict between W2020 and HITRAN2016. In this case, assuming that the label of the lower state is the same, the HITRAN2016 line was attempted to be relabeled to its xMARVEL counterpart. Second, certain HITRAN2016 transitions come only from theoretical sources, without having publicly available experimental counterparts. In this case, obviously, W2020 cannot be utilized to improve the HITRAN2016 dataset. Third, xMARVEL predictions may be considerably more accurate than their HITRAN2016 siblings. In these cases, the line positions should be replaced with the xMARVEL wavenumbers during the next update of HITRAN. Overall, 44 and 329 entries of the H₂¹⁷O and H₂¹⁸O datasets should be reassigned, respectively, while for the rest of the problems found, the third reason applies, and thus, these HITRAN2016 entries should be replaced by their xMARVEL counterparts.

8. Quadrupole-Allowed Transitions

The inclusion of quadrupole-allowed lines in the W2020-H₂¹⁶O dataset, taken from 20CaKaYaKy¹⁵² and 20CaSoSoYa,¹⁵³ strongly affects the structure of the underlying SN. This structural change is manifested in the violation of the bipartite character^{27,28,165} of the original SN formed only by dipole-allowed transitions, making the presence of odd-numbered cycles allowed (note that in bipartite SNs, only even-membered cycles are permitted). This effect should be taken into account during the validation of the rovibrational labels.

Recording extremely weak quadrupole-allowed lines of water vapor is a truly significant success from an experimental (and from a technical) point of view. Nevertheless, the accuracy of the line positions determined in Refs. 152 and 153 is significantly less than either that of recent (CA-)CRDS measurements or our xMARVEL predictions (see Table 6). It can be seen from Table 6 that the uncertainties of the xMARVEL estimates are around 1×10^{-4} cm⁻¹– 2×10^{-4} cm⁻¹, except for one wavenumber derived from NICE-OHMS transitions,¹⁵ which has an accuracy of 6×10^{-7} cm⁻¹, while the deviations between the xMARVEL and the observed values are on the order of 1×10^{-4} cm⁻¹– 7×10^{-3} cm⁻¹. On the one hand, this means that, to date, the quadrupole-allowed line positions of H₂¹⁶O can be determined more precisely in an empirical way than by direct observation, though this situation may change in the near future. On the other hand, the data show that the xMARVEL energy levels are accurate enough to serve as a basis to search for further quadrupole-allowed transitions (the search should be helped with accurate FP quadrupole intensities).

9. Assessment of the Lamb-Dip Data of 10GaFaCaMa

With the appearance of 10GaFaCaMa,³² one of the earliest sets of rovibrational Lamb-dip spectroscopy results became available for water isotopologues. While this study listed only two ultraprecise transitions for H₂¹⁷O, it provided 18 lines for H₂¹⁸O. All these transitions were characterized with an accuracy of 30 kHz,³² in stark contrast to traditional high-resolution spectroscopy measurements, which have uncertainties of 3 MHz–300 MHz, mainly limited by Doppler broadening. It is worth discussing these ground-breaking

TABLE 6. Comparison of quadrupole-allowed transitions of H_2^{16}O reported in $^{20}\text{CaKaYaKy}^{152}$ and $^{20}\text{CaSoSoYa}^{153}$ with their xMARVEL counterparts. The residuals are relative to the xMARVEL predictions

σ_{obs} (cm^{-1})	σ_{xMARVEL} (cm^{-1})	Residual (cm^{-1})	Upper state	Lower state
1819.727	1819.727 66(3)	-0.000 7	(0 1 0) $6_{0,6}$	(0 0 0) $4_{0,4}$
1926.040	1926.039 33(3)	0.000 7	(0 1 0) $9_{0,9}$	(0 0 0) $7_{0,7}$
4032.147	4032.148 23(9)	-0.001 2	(0 0 1) $5_{3,3}$	(0 0 0) $3_{2,1}$
4040.838	4040.838 14(1)	-0.000 1	(0 0 1) $8_{0,8}$	(0 0 0) $6_{1,6}$
4041.450	4041.449 03(5)	0.001 0	(0 0 1) $8_{1,8}$	(0 0 0) $6_{0,6}$
4052.893	4052.895 17(9)	-0.002 2	(0 0 1) $7_{2,6}$	(0 0 0) $5_{1,4}$
4071.454	4071.455 24(1)	-0.001 2	(0 0 1) $6_{3,4}$	(0 0 0) $4_{2,2}$
4083.035	4083.031 18(1)	0.003 8	(0 0 1) $8_{2,7}$	(0 0 0) $6_{1,5}$
4100.719	4100.718 42(9)	0.000 6	(1 0 0) $7_{2,5}$	(0 0 0) $5_{0,5}$
4106.763	4106.762 74(9)	0.000 3	(0 0 1) $7_{3,5}$	(0 0 0) $5_{2,3}$
4108.852	4108.852 77(9)	-0.000 8	(0 0 1) $6_{4,2}$	(0 0 0) $4_{3,2}$
4150.162	4150.162 70(3)	-0.000 7	(0 0 1) $7_{4,4}$	(0 0 0) $5_{3,2}$
7474.6325	7474.635 0(1)	-0.002 5	(1 0 1) $6_{1,5}$	(0 0 0) $4_{2,3}$
7475.4020	7475.400 7(1)	0.001 3	(1 0 1) $5_{2,4}$	(0 0 0) $3_{1,2}$
7488.5747	7488.577 769 9(6)	-0.003 1	(1 0 1) $6_{6,0}$	(0 0 0) $5_{5,0}$
7488.9183	7488.922 4(1)	-0.004 1	(1 0 1) $7_{0,7}$	(0 0 0) $5_{1,5}$
7490.3117	7490.312 1(1)	-0.000 4	(1 0 1) $7_{1,7}$	(0 0 0) $5_{0,5}$
7533.4649	7533.464 4(1)	0.000 5	(1 0 1) $7_{2,6}$	(0 0 0) $5_{1,4}$
7551.7653	7551.764 7(1)	0.000 6	(1 0 1) $9_{1,9}$	(0 0 0) $7_{0,7}$
7581.1247	7581.117 3(2)	0.007 4	(1 0 1) $10_{0,10}$	(0 0 0) $8_{1,8}$
7613.8512	7613.848 8(1)	0.002 4	(1 0 1) $10_{2,9}$	(0 0 0) $8_{1,7}$

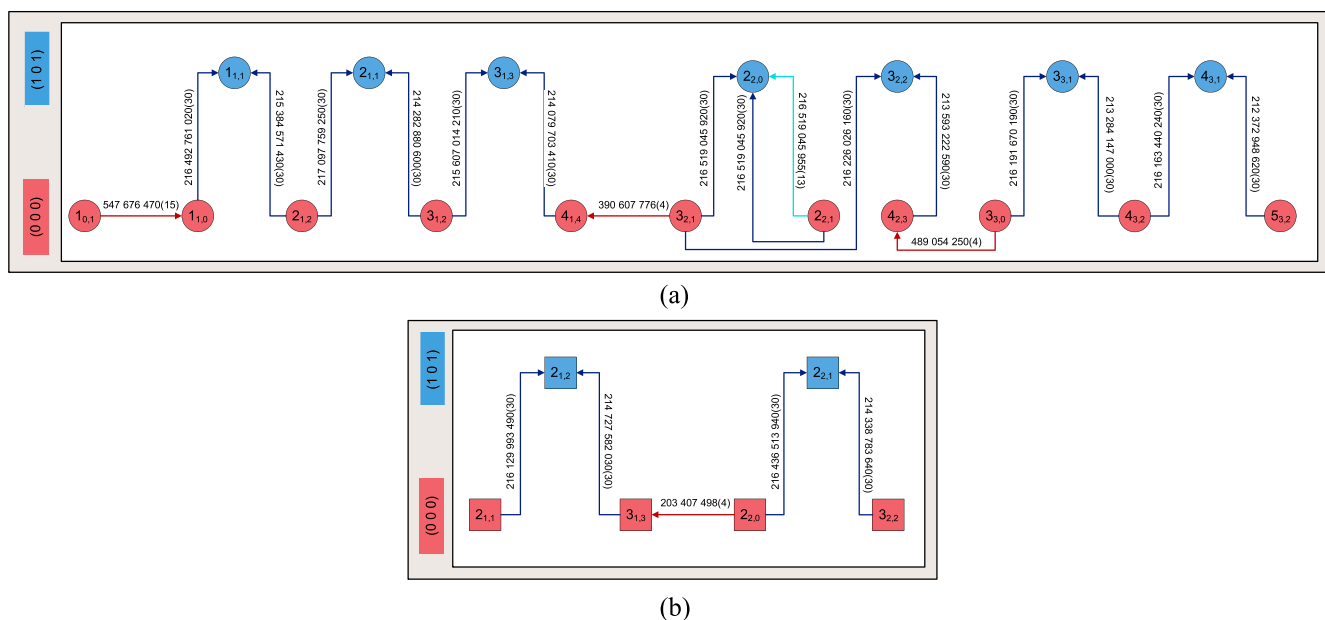
**FIG. 10.** Pictorial representation of all the non-isolated precision measurements performed for *ortho*- [panel (a)] and *para*- H_2^{18}O [panel (b)]. The J_{K_a, K_c} rotational labels within the squares/circles for the *para/ortho* nuclear-spin isomers of H_2^{18}O represent rovibrational states, whose $(v_1 v_2 v_3)$ vibrational labels are indicated in the left-hand-side legend with different colors. Transitions denoted with brown, blue, and cyan arrows are results from $^{06}\text{GoMaGuKn}$,¹¹⁴ $^{10}\text{GaFaCaMa}$,³² and $^{11}\text{GaGaFaCa}$,³⁴ respectively. Lines are associated with their experimental frequencies (in kHz) and the uncertainties of the last few frequency digits (in parentheses).

TABLE 7. Comparison of the 10GaFaCaMa³² lines to their xMARVEL counterparts for H₂¹⁸O

Assignment	$f(10\text{GaFaCaMa})$ (kHz)	$f(\text{xMARVEL})$ (kHz)	Residual (kHz)
(1 0 1) _{4,3,1} ← (0 0 0) _{5,3,2}	212 372 948 620	212 372 948 629	-9
(1 0 1) _{4,3,1} ← (0 0 0) _{4,3,2}	216 163 440 240	216 163 440 231	9
(1 0 1) _{3,3,1} ← (0 0 0) _{4,3,2}	213 284 147 000	213 284 146 983	17
(1 0 1) _{3,3,1} ← (0 0 0) _{3,3,0}	216 191 670 190	216 191 670 207	-17
(1 0 1) _{3,2,2} ← (0 0 0) _{4,2,3}	213 593 222 590	213 593 222 621	-31
(1 0 1) _{3,2,2} ← (0 0 0) _{3,2,1}	216 226 026 160	216 226 026 129	31
(1 0 1) _{2,2,0} ← (0 0 0) _{3,2,1}	214 200 946 980	214 200 946 980	0
(1 0 1) _{2,2,0} ← (0 0 0) _{2,2,1}	216 519 045 920	216 519 045 950	-30
(1 0 1) _{3,1,3} ← (0 0 0) _{4,1,4}	214 079 703 410	214 079 703 428	-18
(1 0 1) _{3,1,3} ← (0 0 0) _{3,1,2}	215 607 014 210	215 607 014 192	18
(1 0 1) _{2,1,1} ← (0 0 0) _{3,1,2}	214 282 880 600	214 282 880 599	1
(1 0 1) _{2,1,1} ← (0 0 0) _{2,1,2}	217 097 759 250	217 097 759 251	-1
(1 0 1) _{2,2,1} ← (0 0 0) _{3,2,2}	214 338 783 640	214 338 783 628	12
(1 0 1) _{2,2,1} ← (0 0 0) _{2,2,0}	216 436 513 940	216 436 513 952	-12
(1 0 1) _{2,1,2} ← (0 0 0) _{3,1,3}	214 727 582 030	214 727 582 001	29
(1 0 1) _{2,1,2} ← (0 0 0) _{2,1,1}	216 129 993 490	216 129 993 519	-29
(1 0 1) _{1,1,1} ← (0 0 0) _{2,1,2}	215 384 571 430	215 384 571 426	4
(1 0 1) _{1,1,1} ← (0 0 0) _{1,1,0}	216 492 761 020	216 492 761 024	-4

TABLE 8. Energy separation between selected pairs of pure rotational levels of H₂¹⁸O

State pair	$\Delta E(10\text{GaFaCaMa}^{32})$ (kHz)	$\Delta E(\text{xMARVEL})$ (kHz)	Residual (kHz)
(0 0 0) _{2,1,2} - (0 0 0) _{1,1,0}	1 108 189 590	1 108 189 597	-7
(0 0 0) _{3,1,3} - (0 0 0) _{2,1,1}	1 402 411 460	1 402 411 517	-57
(0 0 0) _{4,1,4} - (0 0 0) _{3,1,2}	1 527 310 800	1 527 310 764	36
(0 0 0) _{3,2,2} - (0 0 0) _{2,2,0}	2 097 730 300	2 097 730 325	-25
(0 0 0) _{3,2,1} - (0 0 0) _{2,2,1}	2 318 098 940	2 318 098 970	-30
(0 0 0) _{4,2,3} - (0 0 0) _{3,2,1}	2 632 803 570	2 632 803 509	61
(0 0 0) _{3,1,2} - (0 0 0) _{2,1,2}	2 814 878 650	2 814 878 651	-1
(0 0 0) _{4,3,2} - (0 0 0) _{3,3,0}	2 907 523 190	2 907 523 223	-33
(0 0 0) _{5,3,2} - (0 0 0) _{4,3,2}	3 790 491 620	3 790 491 602	18

results for H₂¹⁸O in view of developments in precision spectroscopy¹⁵ and the spectroscopic-network approach.

Figure 10 shows the network formed by the 18 observations for H₂¹⁸O provided by 10GaFaCaMa, all referring to the (0 0 0) and (1 0 1) vibrational states. It is obvious from Fig. 10 that the lines of 10GaFaCaMa form five components without any cycles, making the checking of their internal consistency and precision impossible. Furthermore, these ultraprecise measurements are not connected to the (0 0 0)_{0,0,0} or (0 0 0)_{1,0,1} states, limiting their utility for the extremely precise determination of the underlying energy levels. Fortunately, there are highly accurate transitions from 06GoMaGuKn¹¹⁴ that help connect the states involved in the lines of 10GaFaCaMa. As also clearly shown in Fig. 10, these additional experimental results allow the formation of connected paths with the quite fragmented set of 10GaFaCaMa transitions, allowing the accurate derivation of the *ortho* energy levels [panel (a)] via the extended Ritz principle.¹⁵ As to the *para* path [panel (b) of Fig. 10], further precision-spectroscopy measurements should be designed and performed to connect its starting node [(0 0 0)_{2,1,1}] to the rovibrational ground state.

As the data of Tables 7 and 8 demonstrate, the agreement of the present xMARVEL results is almost perfect not only with the transitions but also with the energy-level separations of 10GaFaCaMa (see Tables 1 and 2 of Ref. 32). It is important to emphasize that in 2011, the (1 0 1)_{2,2,0} ← (0 0 0)_{2,2,1} transition was remeasured and extrapolated to zero pressure, as reported in another paper by the Gianfrani group.³⁴ This newly observed frequency differs from the result of 10GaFaCaMa by 35 kHz, exemplifying how substantial the pressure shift is at this level of precision. The present xMARVEL value agrees with the improved experimental datum³⁴ within 6 kHz.

10. Guiding Atmospheric Simulations

Linelist of water isotopologues are often employed to simulate laboratory as well as “solar” spectra of interest to atmospheric scientists. These simulations require accurate line positions, intensities, widths (broadening, self, and foreign), and shifts (self and foreign). The W2020 database in itself contributes only to the simulation of transition wavenumbers, though it can be straightforwardly

TABLE 9. Number of FP (Ref. 156 for H₂¹⁶O and HotWat78¹²⁸ for H₂¹⁷O and H₂¹⁸O), xMARVEL, and PE transitions of three water isotopologues, with different intensity cutoff values in cm molecule⁻¹. The intensities correspond to room temperature ($T = 296$ K), and those of the minor isotopologues are corrected with their natural terrestrial isotopic abundances. The PE data (also including those levels with existing xMARVEL counterparts) are obtained both with (FG) and without (noFG) the use of the F and G criteria, which are explained in the text

Species	Cutoff	No. of FP	No. of xMARVEL	No. of PE(FG)	No. of PE(noFG)
H ₂ ¹⁶ O	10 ⁻²⁶	35 394	35 349
	10 ⁻²⁷	60 535	58 876
	10 ⁻²⁸	101 646	88 925
	10 ⁻²⁹	168 007	125 882
	10 ⁻³⁰	273 614	171 283
H ₂ ¹⁷ O	10 ⁻²⁶	4 341	4 322	4 339	4 339
	10 ⁻²⁷	8 383	8 085	8 358	8 368
	10 ⁻²⁸	15 535	14 054	15 331	15 426
	10 ⁻²⁹	27 782	22 181	26 548	27 143
	10 ⁻³⁰	48 103	32 407	43 070	45 026
H ₂ ¹⁸ O	10 ⁻²⁶	7 025	7 027	7 025	7 025
	10 ⁻²⁷	13 145	13 117	13 133	13 135
	10 ⁻²⁸	23 674	22 949	23 413	23 505
	10 ⁻²⁹	41 550	36 313	39 410	40 151
	10 ⁻³⁰	70 765	52 501	60 673	63 218

complemented with FP computed intensities. Absorption features due to water vapor are notoriously ubiquitous throughout the extended (far- and near-) infrared region, making knowledge of water lines important on their own right. At the same time, water is the major interferent during the retrieval of other gases in atmospheres.^{166–168} Thus, the spectroscopy of water vapor must be nearly perfect in its own windows, as well as in those windows where gases other than water are retrieved.^{166,168,169} As to our own planet, the amount of water varies several orders of magnitude in the Earth's atmosphere.^{167,170} Therefore, detailed coverage and outstanding line-to-line and window-to-window consistency is needed in water vapor spectroscopy. As seen in Table 9, which provides details about the line position coverage with different absorption intensity cutoff values for H₂¹⁶O, H₂¹⁷O, and H₂¹⁸O, as well as in Figs. 11–15, providing details about spectrum coverage, this is indeed achieved by entries of the W2020 dataset. The linelists of H₂¹⁶O, H₂¹⁷O, and H₂¹⁸O produced during this study are presented in the [supplementary material](#).

The structure and the data of Table 9 need a brief explanation. Taking into account all factors influencing water vapor measurements in the Earth's atmosphere, it is safe to assume that room-temperature absorption intensities smaller than 5×10^{-28} cm molecule⁻¹ are unlikely to be of concern for line-by-line database developers. Then, it is valid to question how complete the W2020 dataset is with respect to different intensity cutoffs for H₂¹⁶O. Of course, minor isotopologues contributing to water spectra should also be considered. The natural abundances of ¹⁶O, ¹⁷O, and ¹⁸O are ~0.9976, 0.0004, and 0.0020, respectively. Of course, enrichment should also be considered if the focus were on laboratory spectra. It is necessary to emphasize that in Table 9, the intensities are corrected for the natural terrestrial isotopic abundances. Then, the data of Table 9 show the total number of transitions with different intensity cutoff values computed *via* accurate FP techniques and the number of

transitions known after the present xMARVEL analyses, with and without PE lines augmenting the xMARVEL data. As seen there, almost all of the lines above 10⁻²⁶ cm molecule⁻¹ are known as a result of the present xMARVEL analyses (more than 99% of the lines are known based on the W2020 data) and more than 60% are empirically available using the cutoff value of 10⁻³⁰ cm molecule⁻¹ for each isotopologue. Thus,

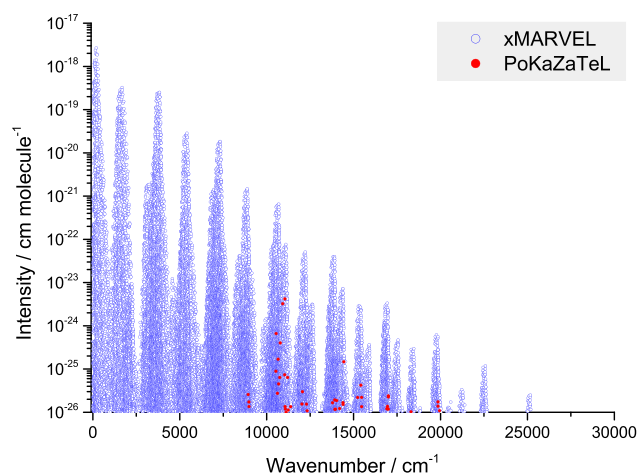


FIG. 11. Room-temperature ($T = 296$ K), one-photon, dipole-allowed H₂¹⁶O linelist up to 30 000 cm⁻¹, with an intensity cutoff of 10⁻²⁶ cm molecule⁻¹, based on xMARVEL line positions and PoKaZaTeL¹⁵⁸ line positions. In the cases where both datasets provide estimates for the same transition wavenumber, only the xMARVEL value is retained in the figure. The intensities are taken from Ref. 156. Completeness of the xMARVEL data is clearly visible.

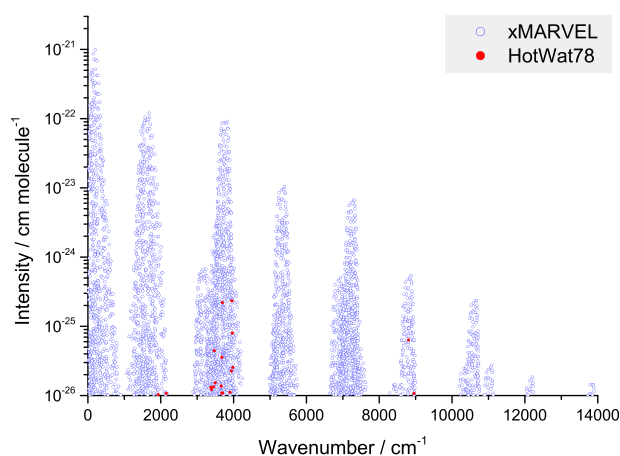


FIG. 12. Room-temperature one-photon, dipole-allowed H_2^{17}O linelist up to $14\,000\text{ cm}^{-1}$, with an intensity cutoff of $10^{-26}\text{ cm molecule}^{-1}$, based on xMARVEL and the HotWat78¹²⁸ line positions. In the cases where both datasets provide estimates for the same transition wavenumber, only the xMARVEL value is retained in the figure. The intensities are taken from Ref. 128.

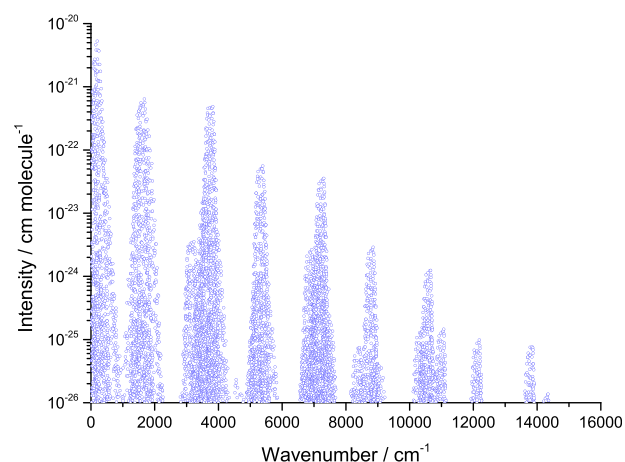


FIG. 14. Room-temperature one-photon, dipole-allowed H_2^{18}O linelist up to $30\,000\text{ cm}^{-1}$, with an intensity cutoff of $10^{-26}\text{ cm molecule}^{-1}$, based on xMARVEL line positions. The intensities are taken from Ref. 128.

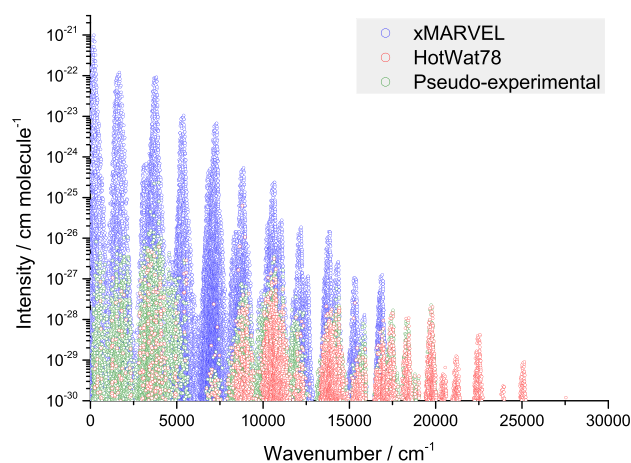


FIG. 13. Room-temperature one-photon, dipole-allowed H_2^{17}O linelist up to $30\,000\text{ cm}^{-1}$, with an intensity cutoff of $10^{-30}\text{ cm molecule}^{-1}$, based on xMARVEL, HotWat78,¹²⁸ and PE line positions. In the cases where a wavenumber is provided by more than one dataset, only the most accurate value is retained in the figure, following the xMARVEL > HotWat78 > PE accuracy relations. The intensities are taken from Ref. 128.

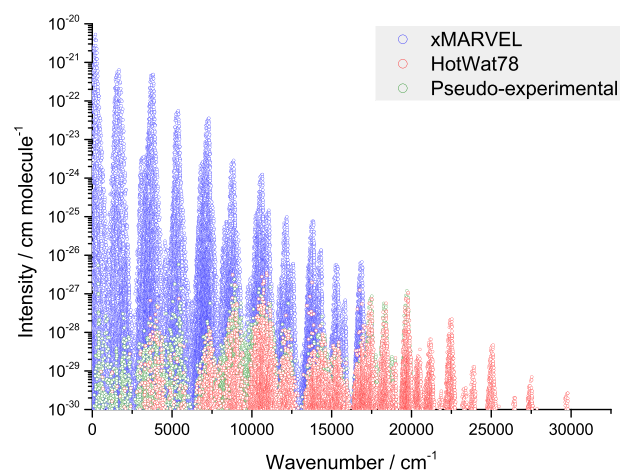


FIG. 15. Room-temperature one-photon, dipole-allowed H_2^{18}O linelist up to $30\,000\text{ cm}^{-1}$, with an intensity cutoff of $10^{-30}\text{ cm molecule}^{-1}$, based on xMARVEL, HotWat78,¹²⁸ and PE line positions. In the cases where a wavenumber is provided by more than one dataset, only the most accurate value is retained in the figure, following the xMARVEL > HotWat78 > PE accuracy relations. The intensities are taken from Ref. 128.

W2020 provides truly remarkable coverage with an outstanding accuracy, as discussed above.

Figures 11–15 display the coverage of water lines based on the W2020 datasets at 296 K. Clearly, with an intensity cutoff of $10^{-26}\text{ cm molecule}^{-1}$, the W2020 dataset can be considered complete for all three water isotopologues. Inclusion of PE lines, based on PE rovibrational energy levels, makes our predictions much more complete in between 10^{-26} and $10^{-30}\text{ cm molecule}^{-1}$. Thus, new experimental results guided by the PE predictions would be highly beneficial for further improving the simulations of water vapor applicable to atmospheric modeling.

11. Summary and Conclusions

The principal results of the present study are the W2020 datasets for three H_2^XO isotopologues ($X = 16, 17, 18$). The W2020 databases contain all rovibrational transitions of these isotopologues collated from the literature, with appropriate labels and uncertainties, as well as empirical energy levels, with well-defined uncertainties, obtained from the measured line positions. The xMARVEL protocol^{30,31} was employed to perform the analysis of the experimental rovibrational transitions of these water isotopologues. xMARVEL was able to validate the great majority of the measurements and yielded a consistent set of uncertainties for the observed transitions and the derived energy values.

The improvements compared to previous extensive compilations^{17,18} available in the literature for these water isotopologues were achieved in several steps. The most important aspects and the consequences of these steps are summarized below.

First, the W2020-H₂¹⁶O dataset³¹ was updated with three relevant sources^{53,63,102} to facilitate the subsequent analysis of the high-resolution spectroscopic data of H₂¹⁷O and H₂¹⁸O. As part of this step, some of the labels in the original W2020-H₂¹⁶O dataset³¹ were changed so that the dataset now mimics considerably better than before (and even supersedes) the limited SISAM¹⁵⁴ and 20MiKa-MoCa⁶⁶ line lists. The most important advantages of the updated W2020-H₂¹⁶O dataset are that (a) it comprises essentially all the transitions accessible within the SISAM dataset, providing the base of the HITRAN2016 line lists, but occasionally with considerably higher accuracy, and (b) it shows full agreement with the lines of Ref. 66 with significant absorption intensities.

Second, all sources published after 2010 on high-resolution spectra of H₂¹⁷O and H₂¹⁸O were gathered and added to the W2020 dataset together with the results of those studies missed during the compilation of the TG-H₂¹⁷O and TG-H₂¹⁸O databases.^{16,17} Due to this comprehensive search, 35 and 37 new experimental sources were appended to the TG-H₂¹⁷O and TG-H₂¹⁸O line catalogs, respectively. The W2020-H₂¹⁷O list consists of 27 045 transitions, yielding 5278 empirical energies with statistically dependable uncertainties. Although the W2020-H₂¹⁷O database became three times larger than the original TG-H₂¹⁷O collection, the number of empirical energy values determined by these transitions increased only twofold, while the number of newly derived energy levels is even less favorable for H₂¹⁸O. The W2020-H₂¹⁸O dataset contains 66 166 transitions; thus, it is about twice as large as its parent TG database.¹⁷ Nevertheless, the number of accurately deduced empirical energy levels increased from 5133 to only 6865. These statistics are not only important in themselves, but they also provide a warning to spectroscopists that there is considerable room to improve the design of high-resolution experiments if the goal is to extend our knowledge about the rovibrational energy levels of water isotopologues (needless to say, the same holds for all molecules).

The empirical energies of the W2020 datasets allowed the creation of accurate line lists with well-defined uncertainties for all three H₂^XO isotopologues, which represent one of the most significant results of the present study. It must also be mentioned that the overwhelming majority of the theoretical lines are associated with xMARVEL predictions for all three species considered, providing a much improved coverage compared to the empirical information extracted from the previous TG-H₂^XO databases.^{16–20} The rovibrational states unknown from experiments but necessary to obtain full coverage are listed, together with their approximate energies, in the [supplementary material](#).

Third, a concerted effort was made to “optimize” the uncertainties attached to the observed lines entering the xMARVEL analysis. This means that the uncertainties were decreased as much as feasible within certain experimental limitations. The upgraded uncertainties are utilized to classify the transitions of a particular source into segments,³⁰ as required by the xMARVEL protocol. Note that xMARVEL is capable of retaining the accuracy of the most precise experimental lines during the xMARVEL analysis and transferring

that to the empirical energy values to the maximal extent allowed by the deviations of the line positions.

Fourth, the best set of consistent labels was created for the rovibrational states of the H₂^XO isotopologues, synchronizing the H₂¹⁷O and H₂¹⁸O labels with their W2020-H₂¹⁶O counterparts. Therefore, we believe that, whenever possible, the labels of the rovibrational states included in the three W2020-H₂^XO databases are consistent with each other.

Fifth, based on trends characterizing the differences (residuals) of FP and empirical energies for the various H₂^XO isotopologues, so-called PE energy values¹²⁸ were derived, which provide enhanced accuracy for yet-to-be-observed rovibrational states of H₂¹⁷O and H₂¹⁸O. These PE levels, whose accuracy should be close to that of standard FT-IR measurements, can be employed to supplement the empirical energies coming from the xMARVEL procedure. When PE levels are involved in the generation of spectra based on W2020 energies, a considerably improved coverage can be obtained, especially for the visible part of the water spectra, where whole new bands appear (with intensities below 10^{−28} cm molecule^{−1}). It must be noted that during the course of this work, a small number of so far unobserved H₂¹⁶O levels were identified, which could also be determined using the PE scheme, by inverting the parent–daughter roles of the water species. These H₂¹⁶O energy levels will be presented elsewhere, alongside an analysis of what matching these levels for different isotopologues tells us about limits of the Born–Oppenheimer approximation.

As to the final conclusion of this study, we recommend that both the validated rovibrational transitions and the accurate empirical energy levels of this study should be included in the next generation of line-by-line spectroscopic information systems, such as HITRAN.⁴

12. Supplementary Material

See the [supplementary material](#) for lists of transitions and energy levels characterizing the W2020 dataset of H₂¹⁶O, H₂¹⁷O, and H₂¹⁸O, as well as for PE levels of H₂¹⁷O and H₂¹⁸O and the problematic transitions of the SISAM dataset and the HITRAN2016 information system. A room-temperature line list based principally on empirical (xMARVEL) energy levels is also provided, employing an intensity cutoff of 10^{−30} cm molecule^{−1}.

Acknowledgments

The work performed in Budapest received support from NKFIH (Grant No. K119658), from the ELTE Institutional Excellence Program (Grant No. TKP2020-IKA-05) financed by the Hungarian Ministry of Human Capacities, and from the grant VEKOP-2.3.2-16-2017-000. The work performed in the United Kingdom received support from the UK Natural Environment Research Council (NERC) through Grant No. NE/T000767/1 and from the European Research Council (ERC) under the European Union’s Horizon 2020 research and innovation programme through Advance Grant No. 883830. The joint work between the Budapest and London groups received support from the COST Action MOLIM (Molecules in Motion, CM1405), also in the form of a Short Term Scientific Mission (STSM) awarded to A.G.C. The work performed by A.A.K. and R.I.O. was supported by State Project IAP RAS No. 0035-2019-0016. O.L.P. and N.F.Z. were funded by RFBR under Project No. 18-02-00577. Dr.

Eamon Conway is thanked for fruitful discussions concerning the HITRAN datasets of H₂¹⁶O, H₂¹⁷O, and H₂¹⁸O.

13. Data Availability

The data that support the findings of this study are available within the article and its [supplementary material](#) and on the ReSpecTh website at <http://ReSpecTh.hu>.

14. References

- ¹R. P. Wayne, *Chemistry of Atmospheres*, 3rd ed. (Oxford University Press, New York, 2000).
- ²P. F. Bernath, *Phys. Chem. Chem. Phys.* **4**, 1501 (2002).
- ³C. D. Boone, K. A. Walker, and P. F. Bernath, *J. Quant. Spectrosc. Radiat. Transfer* **105**, 525 (2007).
- ⁴I. E. Gordon, L. S. Rothman, C. Hill, R. V. Kochanov, Y. Tan, P. F. Bernath, M. Birk, V. Boudon, A. Campargue, K. V. Chance, B. J. Drouin, J.-M. Flaud, R. R. Gamache, J. T. Hodges, D. Jacquemart, V. I. Perevalov, A. Perrin, K. P. Shine, M.-A. H. Smith, J. Tennyson, G. C. Toon, H. Tran, V. G. Tyuterev, A. Barbe, A. G. Császár, V. M. Devi, T. Furtenbacher, J. J. Harrison, J.-M. Hartmann, A. Jolly, T. J. Johnson, T. Karman, I. Kleiner, A. A. Kyuberis, J. Loos, O. M. Lyulin, S. T. Massie, S. N. Mikhailenko, N. Moazzen-Ahmadi, H. S. P. Müller, O. V. Naumenko, A. V. Nikitin, O. L. Polyansky, M. Rey, M. Rotger, S. W. Sharpe, K. Sung, E. Starikova, S. A. Tashkun, J. Vander Auwera, G. Wagner, J. Wilzewski, P. Wcisło, S. Yu, and E. J. Zak, *J. Quant. Spectrosc. Radiat. Transfer* **203**, 3 (2017).
- ⁵J. L. Hall, *Rev. Mod. Phys.* **78**, 1279 (2006).
- ⁶T. W. Hänsch, *Rev. Mod. Phys.* **78**, 1297 (2006).
- ⁷*Handbook of High-Resolution Spectroscopy*, edited by M. Quack and F. Merkt (Wiley, New York, 2014).
- ⁸S. Twagirayezu, M. J. Cich, T. J. Sears, C. P. McRaven, and G. E. Hall, *J. Mol. Spectrosc.* **316**, 64 (2015).
- ⁹L. Santamaria, V. Di Sarno, P. De Natale, M. De Rosa, M. Inguscio, S. Mosca, I. Ricciardi, D. Calonico, F. Levi, and P. Maddaloni, *Phys. Chem. Chem. Phys.* **18**, 16715 (2016).
- ¹⁰D. Gatti, R. Gotti, A. Gambetta, M. Belmonte, G. Galzerano, P. Laporta, and M. Marangoni, *Sci. Rep.* **6**, 27183 (2016).
- ¹¹J. Wang, Y. R. Sun, L.-G. Tao, A.-W. Liu, T.-P. Hua, F. Meng, and S.-M. Hu, *Rev. Sci. Instrum.* **88**, 043108 (2017).
- ¹²Z. D. Reed, D. A. Long, H. Fleurbaey, and J. T. Hodges, *Optica* **7**, 1209 (2020).
- ¹³K. Pachucki and J. Komasa, *Phys. Chem. Chem. Phys.* **12**, 9188 (2010).
- ¹⁴A. G. Császár, C. Fábri, T. Szidarovszky, E. Mátyus, T. Furtenbacher, and G. Czakó, *Phys. Chem. Chem. Phys.* **14**, 1085 (2012).
- ¹⁵R. Tóbiás, T. Furtenbacher, I. Simkó, A. G. Császár, M. L. Diouf, F. M. J. Cozijn, J. M. A. Staa, E. J. Salumbides, and W. Ubachs, *Nat. Commun.* **11**, 1708 (2020).
- ¹⁶J. Tennyson, P. F. Bernath, L. R. Brown, A. Campargue, M. R. Carleer, A. G. Császár, R. R. Gamache, J. T. Hodges, A. Jenouvrier, O. V. Naumenko, O. L. Polyansky, L. S. Rothman, R. A. Toth, A. C. Vandaele, N. F. Zobov, L. Daumont, A. Z. Fazliev, T. Furtenbacher, I. E. Gordon, S. N. Mikhailenko, and S. V. Shirin, *J. Quant. Spectrosc. Radiat. Transfer* **110**, 573 (2009).
- ¹⁷J. Tennyson, P. F. Bernath, L. R. Brown, A. Campargue, A. G. Császár, L. Daumont, R. R. Gamache, J. T. Hodges, O. V. Naumenko, O. L. Polyansky, L. S. Rothman, R. A. Toth, A. C. Vandaele, N. F. Zobov, S. Fally, A. Z. Fazliev, T. Furtenbacher, I. E. Gordon, S.-M. Hu, S. N. Mikhailenko, and B. A. Voronin, *J. Quant. Spectrosc. Radiat. Transfer* **111**, 2160 (2010).
- ¹⁸J. Tennyson, P. F. Bernath, L. R. Brown, A. Campargue, A. G. Császár, L. Daumont, R. R. Gamache, J. T. Hodges, O. V. Naumenko, O. L. Polyansky, L. S. Rothman, A. C. Vandaele, N. F. Zobov, A. R. Al Derzi, C. Fábri, A. Z. Fazliev, T. Furtenbacher, I. E. Gordon, L. Lodi, and I. I. Mizus, *J. Quant. Spectrosc. Radiat. Transfer* **117**, 29 (2013).
- ¹⁹J. Tennyson, P. F. Bernath, L. R. Brown, A. Campargue, A. G. Császár, L. Daumont, R. R. Gamache, J. T. Hodges, O. V. Naumenko, O. L. Polyansky, L. S. Rothman, A. C. Vandaele, N. F. Zobov, N. Dénes, A. Z. Fazliev, T. Furtenbacher, I. E. Gordon, S.-M. Hu, T. Szidarovszky, and I. A. Vasilenko, *J. Quant. Spectrosc. Radiat. Transfer* **142**, 93 (2014).
- ²⁰J. Tennyson, P. F. Bernath, L. R. Brown, A. Campargue, A. G. Császár, L. Daumont, R. R. Gamache, J. T. Hodges, O. V. Naumenko, O. L. Polyansky, L. S. Rothman, A. C. Vandaele, and N. F. Zobov, *Pure Appl. Chem.* **86**, 71 (2014).
- ²¹A. G. Császár, G. Czakó, T. Furtenbacher, and E. Mátyus, *Annu. Rep. Comput. Chem.* **3**, 155 (2007).
- ²²T. Furtenbacher, A. G. Császár, and J. Tennyson, *J. Mol. Spectrosc.* **245**, 115 (2007).
- ²³T. Furtenbacher and A. G. Császár, *J. Quant. Spectrosc. Radiat. Transfer* **109**, 1234 (2008).
- ²⁴A. G. Császár and T. Furtenbacher, *J. Mol. Spectrosc.* **266**, 99 (2011).
- ²⁵T. Furtenbacher and A. G. Császár, *J. Quant. Spectrosc. Radiat. Transfer* **113**, 929 (2012).
- ²⁶T. Furtenbacher and A. G. Császár, “The role of intensities in determining characteristics of spectroscopic networks,” *J. Mol. Spectrosc.* **1009**, 123 (2012).
- ²⁷T. Furtenbacher, P. Árendás, G. Mellau, and A. G. Császár, *Sci. Rep.* **4**, 4654 (2014).
- ²⁸A. G. Császár, T. Furtenbacher, and P. Árendás, *J. Phys. Chem. A* **120**, 8949 (2016).
- ²⁹R. Tóbiás, T. Furtenbacher, and A. G. Császár, *J. Quant. Spectrosc. Radiat. Transfer* **203**, 557 (2017).
- ³⁰R. Tóbiás, T. Furtenbacher, J. Tennyson, and A. G. Császár, *Phys. Chem. Chem. Phys.* **21**, 3473 (2019).
- ³¹T. Furtenbacher, R. Tóbiás, J. Tennyson, O. L. Polyansky, and A. G. Császár, *J. Phys. Chem. Ref. Data* **49**, 033101 (2020).
- ³²A. Gambetta, E. Fasci, A. Castrillo, M. Marangoni, G. Galzerano, G. Casa, P. Laporta, and L. Gianfrani, *New J. Phys.* **12**, 103006 (2010).
- ³³S. Béguier, S. Mikhailenko, and A. Campargue, *J. Mol. Spectrosc.* **265**, 106 (2011).
- ³⁴G. Galzerano, A. Gambetta, E. Fasci, A. Castrillo, M. Marangoni, P. Laporta, and L. Gianfrani, *Appl. Phys. B* **102**, 725 (2011).
- ³⁵M. A. Koshelev, *J. Quant. Spectrosc. Radiat. Transfer* **112**, 550 (2011).
- ³⁶O. M. Leshchishina, O. V. Naumenko, and A. Campargue, *J. Mol. Spectrosc.* **268**, 28 (2011).
- ³⁷O. M. Leshchishina, O. V. Naumenko, and A. Campargue, *J. Quant. Spectrosc. Radiat. Transfer* **112**, 913 (2011).
- ³⁸S. Mikhailenko, S. Kassi, L. Wang, and A. Campargue, *J. Mol. Spectrosc.* **269**, 92 (2011).
- ³⁹M. J. Down, J. Tennyson, J. Orphal, P. Chelin, and A. A. Ruth, *J. Mol. Spectrosc.* **282**, 1 (2012).
- ⁴⁰O. Leshchishina, S. Mikhailenko, D. Mondelain, S. Kassi, and A. Campargue, *J. Quant. Spectrosc. Radiat. Transfer* **113**, 2155 (2012).
- ⁴¹S. N. Mikhailenko, O. V. Naumenko, A. V. Nikitin, I. A. Vasilenko, A.-W. Liu, K.-F. Song, H.-Y. Ni, and S.-M. Hu, *J. Quant. Spectrosc. Radiat. Transfer* **113**, 653 (2012).
- ⁴²C. Oudot, L. Régalia, S. Mikhailenko, X. Thomas, P. Von Der Heyden, and D. Décatoire, *J. Quant. Spectrosc. Radiat. Transfer* **113**, 859 (2012).
- ⁴³S. S. Vasilchenko, S. N. Mikhailenko, V. I. Serdyukov, and L. N. Sinita, *Opt. Spectrosc.* **113**, 499 (2012).
- ⁴⁴O. Leshchishina, S. N. Mikhailenko, D. Mondelain, S. Kassi, and A. Campargue, *J. Quant. Spectrosc. Radiat. Transfer* **130**, 69 (2013).
- ⁴⁵S. N. Mikhailenko, V. I. Serdyukov, L. N. Sinita, and S. S. Vasilchenko, *Opt. Spectrosc.* **115**, 912 (2013).
- ⁴⁶A.-W. Liu, O. V. Naumenko, S. Kassi, and A. Campargue, *J. Quant. Spectrosc. Radiat. Transfer* **138**, 97 (2014).
- ⁴⁷L. Regalia, C. Oudot, S. Mikhailenko, L. Wang, X. Thomas, A. Jenouvrier, and P. Von der Heyden, *J. Quant. Spectrosc. Radiat. Transfer* **136**, 119 (2014).
- ⁴⁸A. Campargue, S. N. Mikhailenko, B. G. Lohan, E. V. Karlovets, D. Mondelain, and S. Kassi, *J. Quant. Spectrosc. Radiat. Transfer* **157**, 135 (2015).
- ⁴⁹S. N. Mikhailenko, V. I. Serdyukov, and L. N. Sinita, *J. Quant. Spectrosc. Radiat. Transfer* **156**, 36 (2015).
- ⁵⁰L. H. Coudert and P. Chelin, *J. Mol. Spectrosc.* **326**, 130 (2016).

- ⁵¹S. N. Mikhailenko, O. Leshchishina, E. V. Karlovets, D. Mondelain, S. Kassi, and A. Campargue, *J. Quant. Spectrosc. Radiat. Transfer* **177**, 108 (2016).
- ⁵²M. Birk, G. Wagner, J. Loos, L. Lodi, O. L. Polyansky, A. A. Kyuberis, N. F. Zobov, and J. Tennyson, *J. Quant. Spectrosc. Radiat. Transfer* **203**, 88 (2017).
- ⁵³A. Campargue, S. N. Mikhailenko, S. Vasilchenko, C. Reynaud, S. Béguier, P. Cermák, D. Mondelain, S. Kassi, and D. Romanini, *J. Quant. Spectrosc. Radiat. Transfer* **189**, 407 (2017).
- ⁵⁴J. Loos, M. Birk, and G. Wagner, *J. Quant. Spectrosc. Radiat. Transfer* **203**, 103 (2017).
- ⁵⁵D. Mondelain, S. N. Mikhailenko, E. V. Karlovets, S. Béguier, S. Kassi, and A. Campargue, *J. Quant. Spectrosc. Radiat. Transfer* **203**, 206 (2017).
- ⁵⁶S. N. Mikhailenko, D. Mondelain, E. V. Karlovets, S. Kassi, and A. Campargue, *J. Quant. Spectrosc. Radiat. Transfer* **206**, 163 (2018).
- ⁵⁷S. N. Mikhailenko, V. I. Serdyukov, and L. N. Sinitsa, *J. Quant. Spectrosc. Radiat. Transfer* **217**, 170 (2018).
- ⁵⁸Y. Tan, S. N. Mikhailenko, J. Wang, A.-W. Liu, X.-Q. Zhao, G.-L. Liu, and S.-M. Hu, *J. Quant. Spectrosc. Radiat. Transfer* **221**, 233 (2018).
- ⁵⁹A.-W. Liu, G.-L. Liu, X.-Q. Zhao, J. Wang, Y. Tan, and S.-M. Hu, *J. Quant. Spectrosc. Radiat. Transfer* **239**, 106651 (2019).
- ⁶⁰S. N. Mikhailenko, E. V. Karlovets, S. Vasilchenko, D. Mondelain, S. Kassi, and A. Campargue, *J. Quant. Spectrosc. Radiat. Transfer* **236**, 106574 (2019).
- ⁶¹S. N. Mikhailenko, D. Mondelain, E. V. Karlovets, S. Kassi, and A. Campargue, *J. Quant. Spectrosc. Radiat. Transfer* **222-223**, 229 (2019).
- ⁶²L. Régalia, X. Thomas, T. Rennesson, and S. Mikhailenko, *J. Quant. Spectrosc. Radiat. Transfer* **235**, 257 (2019).
- ⁶³S. N. Mikhailenko, S. Béguier, T. A. Odintsova, M. Yu. Tretyakov, O. Pirali, and A. Campargue, *J. Quant. Spectrosc. Radiat. Transfer* **253**, 107105 (2020).
- ⁶⁴L. N. Sinitsa, V. I. Serdyukov, E. R. Polovtseva, A. D. Bykov, and A. P. Scherbakov, *J. Quant. Spectrosc. Radiat. Transfer* **246**, 106916 (2020).
- ⁶⁵I. A. Vasilenko, O. V. Naumenko, V. I. Serdyukov, and L. N. Sinitsa, *J. Quant. Spectrosc. Radiat. Transfer* **253**, 107101 (2020).
- ⁶⁶S. N. Mikhailenko, S. Kassi, D. Mondelain, and A. Campargue, *J. Quant. Spectrosc. Radiat. Transfer* **245**, 106840 (2020).
- ⁶⁷W. S. Benedict, M. A. Pollack, and W. J. Tomlinson III, *IEEE J. Quantum Electron.* **5**, 108 (1969).
- ⁶⁸P. E. Fraley, K. Narahari Rao, and L. H. Jones, *J. Mol. Spectrosc.* **29**, 312 (1969).
- ⁶⁹F. X. Powell and D. R. Johnson, *Phys. Rev. Lett.* **24**, 637 (1970).
- ⁷⁰G. Steenbeckeliers and J. Bellet, *C. R. Acad. Sci. Paris* **273**, 471 (1971).
- ⁷¹J. G. Williamson, K. Narahari Rao, and L. H. Jones, *J. Mol. Spectrosc.* **40**, 372 (1971).
- ⁷²F. C. D. Lucia, P. Helminger, R. L. Cook, and W. Gordy, *Phys. Rev. A* **6**, 1324 (1972).
- ⁷³C. Camy-Peyret, J. M. Flaud, G. Guelachvili, and C. Amiot, *Mol. Phys.* **26**, 825 (1973).
- ⁷⁴F. C. D. Lucia and P. Helminger, *J. Mol. Spectrosc.* **56**, 138 (1975).
- ⁷⁵J. W. Fleming and M. J. Gibson, *J. Mol. Spectrosc.* **62**, 326 (1976).
- ⁷⁶R. A. Toth, J. M. Flaud, and C. Camy-Peyret, *J. Mol. Spectrosc.* **67**, 185 (1977).
- ⁷⁷R. A. Toth, J.-M. Flaud, and C. Camy-Peyret, *J. Mol. Spectrosc.* **67**, 206 (1977).
- ⁷⁸F. Winther, *J. Mol. Spectrosc.* **65**, 405 (1977).
- ⁷⁹J. W. C. Johns and A. R. W. McKellar, *Can. J. Phys.* **56**, 737 (1978).
- ⁸⁰J. Kauppinen, T. Kärkkäinen, and E. Kyrö, *J. Mol. Spectrosc.* **71**, 15 (1978).
- ⁸¹C. Camy-Peyret, J.-M. Flaud, and N. Papineau, *C. R. Acad. Sci. Paris* **290B**, 537 (1980).
- ⁸²J. Kauppinen and E. Kyrö, *J. Mol. Spectrosc.* **84**, 405 (1980).
- ⁸³R. H. Partridge, *J. Mol. Spectrosc.* **87**, 429 (1981).
- ⁸⁴G. Guelachvili, *J. Opt. Soc. Am.* **73**, 137 (1983).
- ⁸⁵A. S. Pine, M. J. Coulombe, C. Camy-Peyret, and J.-M. Flaud, *J. Phys. Chem. Ref. Data* **12**, 413 (1983).
- ⁸⁶R. A. Toth and J. W. Brault, *Appl. Opt.* **22**, 908 (1983).
- ⁸⁷J.-P. Chevillard, J.-Y. Mandin, J.-M. Flaud, and C. Camy-Peyret, *Can. J. Phys.* **63**, 1112 (1985).
- ⁸⁸J. W. C. Johns, *J. Opt. Soc. Am. B* **2**, 1340 (1985).
- ⁸⁹J.-P. Chevillard, J.-Y. Mandin, C. Camy-Peyret, and J.-M. Flaud, *Can. J. Phys.* **64**, 746 (1986).
- ⁹⁰J.-P. Chevillard, J.-Y. Mandin, J.-M. Flaud, and C. Camy-Peyret, *J. Quant. Spectrosc. Radiat. Transfer* **36**, 395 (1986).
- ⁹¹S. P. Belov, I. N. Kozin, O. L. Polyansky, M. Y. Tretyakov, and N. F. Zobov, *J. Mol. Spectrosc.* **126**, 113 (1987).
- ⁹²J.-P. Chevillard, J.-Y. Mandin, J.-M. Flaud, and C. Camy-Peyret, *Can. J. Phys.* **65**, 777 (1987).
- ⁹³R. A. Toth, *J. Opt. Soc. Am. B* **9**, 462 (1992).
- ⁹⁴R. A. Toth, *J. Opt. Soc. Am. B* **10**, 1526 (1993).
- ⁹⁵R. A. Toth, *J. Mol. Spectrosc.* **166**, 184 (1994).
- ⁹⁶R. A. Toth, *Appl. Opt.* **33**, 4868 (1994).
- ⁹⁷A. Bykov, O. Naumenko, T. Petrova, A. Scherbakov, L. Sinitsa, J. Y. Mandin, C. Camy-Peyret, and J.-M. Flaud, *J. Mol. Spectrosc.* **172**, 243 (1995).
- ⁹⁸R. A. Toth, *J. Mol. Spectrosc.* **190**, 379 (1998).
- ⁹⁹C. Camy-Peyret, J.-M. Flaud, J.-Y. Mandin, A. Bykov, O. Naumenko, L. Sinitsa, and B. Voronin, *J. Quant. Spectrosc. Radiat. Transfer* **61**, 795 (1999).
- ¹⁰⁰F. Matsushima, H. Nagase, T. Nakauchi, H. Odashima, and K. Takagi, *J. Mol. Spectrosc.* **193**, 217 (1999).
- ¹⁰¹L. Moretti, A. Sasso, L. Gianfrani, and R. Ciurylo, *J. Mol. Spectrosc.* **205**, 20 (2001).
- ¹⁰²H. Naus, W. Ubachs, P. F. Levelt, O. L. Polyansky, N. F. Zobov, and J. Tennyson, *J. Mol. Spectrosc.* **205**, 117 (2001).
- ¹⁰³S. N. Mikhailenko, V. G. Tyuterev, V. I. Starikov, K. K. Albert, B. P. Winnewisser, M. Winnewisser, G. Mellau, C. Camy-Peyret, R. Lanquetin, J.-M. Flaud, and J. W. Brault, *J. Mol. Spectrosc.* **213**, 91 (2002).
- ¹⁰⁴R. Schermaul, R. C. M. Learner, A. A. D. Canas, J. W. Brault, O. L. Polyansky, D. Belmiloud, N. F. Zobov, and J. Tennyson, *J. Mol. Spectrosc.* **211**, 169 (2002).
- ¹⁰⁵M. Tanaka, J. W. Brault, and J. Tennyson, *J. Mol. Spectrosc.* **216**, 77 (2002).
- ¹⁰⁶S. N. Mikhailenko, V. G. Tyuterev, and G. Mellau, *J. Mol. Spectrosc.* **217**, 195 (2003).
- ¹⁰⁷R. N. Tolchenov, J. Tennyson, S. V. Shirin, N. F. Zobov, O. L. Polyansky, and A. N. Maurellis, *J. Mol. Spectrosc.* **221**, 99 (2003).
- ¹⁰⁸P. Macko, D. Romanini, S. N. Mikhailenko, O. V. Naumenko, S. Kassi, A. Jenouvrier, V. G. Tyuterev, and A. Campargue, *J. Mol. Spectrosc.* **227**, 90 (2004).
- ¹⁰⁹M. Tanaka, M. Sneep, W. Ubachs, and J. Tennyson, *J. Mol. Spectrosc.* **226**, 1 (2004).
- ¹¹⁰M. Tanaka, O. Naumenko, J. W. Brault, and J. Tennyson, *J. Mol. Spectrosc.* **234**, 1 (2005).
- ¹¹¹R. N. Tolchenov, O. Naumenko, N. F. Zobov, S. V. Shirin, O. L. Polyansky, J. Tennyson, M. Carleer, P.-F. Coheur, S. Fally, A. Jenouvrier, and A. C. Vandaele, *J. Mol. Spectrosc.* **233**, 68 (2005).
- ¹¹²R. N. Tolchenov and J. Tennyson, *J. Mol. Spectrosc.* **231**, 23 (2005).
- ¹¹³R. A. Toth, *J. Quant. Spectrosc. Radiat. Transfer* **94**, 51 (2005).
- ¹¹⁴G. Y. Golubiatnikov, V. N. Markov, A. Guarnieri, and R. Knochel, *J. Mol. Spectrosc.* **240**, 191 (2006).
- ¹¹⁵L. Joly, B. Parvitte, V. Zéninari, D. Courtois, and G. Durré, *J. Quant. Spectrosc. Radiat. Transfer* **102**, 129 (2006).
- ¹¹⁶A.-W. Liu, J.-H. Du, K.-F. Song, L. Wang, L. Wan, and S.-M. Hu, *J. Mol. Spectrosc.* **237**, 149 (2006).
- ¹¹⁷A.-W. Liu, S.-M. Hu, C. Camy-Peyret, J.-Y. Mandin, O. Naumenko, and B. Voronin, *J. Mol. Spectrosc.* **237**, 53 (2006).
- ¹¹⁸A.-W. Liu, O. Naumenko, K.-F. Song, B. Voronin, and S.-M. Hu, *J. Mol. Spectrosc.* **236**, 127 (2006).
- ¹¹⁹F. Mazzotti, O. V. Naumenko, S. Kassi, A. D. Bykov, and A. Campargue, *J. Mol. Spectrosc.* **239**, 174 (2006).
- ¹²⁰O. Naumenko, M. Sneep, M. Tanaka, S. V. Shirin, W. Ubachs, and J. Tennyson, *J. Mol. Spectrosc.* **237**, 63 (2006).
- ¹²¹A. Jenouvrier, L. Daumont, L. Régalia-Jarlot, V. G. Tyuterev, M. Carleer, A. C. Vandaele, S. Mikhailenko, and S. Fally, *J. Quant. Spectrosc. Radiat. Transfer* **105**, 326 (2007).
- ¹²²F. Mazzotti, R. N. Tolchenov, and A. Campargue, *J. Mol. Spectrosc.* **243**, 78 (2007).

- ¹²⁵S. N. Mikhailenko, W. Le, S. Kassi, and A. Campargue, *J. Mol. Spectrosc.* **244**, 170 (2007).
- ¹²⁶O. V. Naumenko, B. A. Voronin, F. Mazzotti, J. Tennyson, and A. Campargue, *J. Mol. Spectrosc.* **248**, 122 (2008).
- ¹²⁷R. Tolchenov and J. Tennyson, *J. Quant. Spectrosc. Radiat. Transfer* **109**, 559 (2008).
- ¹²⁸A. Liu, O. Naumenko, S. Kassi, and A. Campargue, *J. Quant. Spectrosc. Radiat. Transfer* **110**, 1781 (2009).
- ¹²⁹C. Puzzarini, G. Cazzoli, M. E. Harding, J. Vázquez, and J. Gauss, *J. Chem. Phys.* **131**, 234304 (2009).
- ¹³⁰O. L. Polyansky, A. A. Kyuberis, L. Lodi, J. Tennyson, S. N. Yurchenko, R. I. Ovsyannikov, and N. F. Zobov, *Mon. Not. R. Astron. Soc.* **466**, 1363 (2017).
- ¹³¹X. Huang, D. W. Schwenke, and T. J. Lee, *J. Quant. Spectrosc. Radiat. Transfer* **230**, 222 (2019).
- ¹³²L. K. McKemmish, T. Masseron, H. J. Hoeijmakers, V. Pérez-Mesa, S. L. Grimm, S. N. Yurchenko, and J. Tennyson, *Mon. Not. R. Astron. Soc.* **488**, 2836 (2019).
- ¹³³Ya. V. Pavlenko, S. N. Yurchenko, L. K. McKemmish, and J. Tennyson, *Astron. Astrophys.* **642**, A77 (2020).
- ¹³⁴A. Miani and J. Tennyson, *J. Chem. Phys.* **120**, 2732 (2004).
- ¹³⁵M. E. J. Newman, *Networks* (Oxford University Press, Oxford, 2000).
- ¹³⁶J.-M. Flaud, C. Camy-Peyret, and J. P. Maillard, *Mol. Phys.* **32**, 499 (1976).
- ¹³⁷S. A. Tashkun, V. I. Perevalov, J.-L. Teffo, A. D. Bykov, and N. N. Lavrentieva, *J. Quant. Spectrosc. Radiat. Transfer* **82**, 165 (2003).
- ¹³⁸N. Åslund, *J. Mol. Spectrosc.* **50**, 424 (1974).
- ¹³⁹T. Furtenbacher, I. Szabó, A. G. Császár, P. F. Bernath, S. N. Yurchenko, and J. Tennyson, *Astrophys. J. Suppl. Ser.* **224**, 44 (2016).
- ¹⁴⁰L. K. McKemmish, T. Masseron, S. Sheppard, E. Sandeman, Z. Schofield, T. Furtenbacher, A. G. Császár, J. Tennyson, and C. Sousa-Silva, *Astrophys. J. Suppl. Ser.* **228**, 15 (2017).
- ¹⁴¹L. K. McKemmish, J. Borsovszky, K. L. Goodhew, S. Sheppard, A. F. V. Bennett, A. D. J. Martin, A. Singh, C. A. J. Sturgeon, T. Furtenbacher, A. G. Császár, and J. Tennyson, *Astrophys. J.* **867**, 33 (2018).
- ¹⁴²D. Darby-Lewis, H. Shah, D. Joshi, F. Khan, M. Kauwo, N. Sethi, P. F. Bernath, T. Furtenbacher, R. Tóbiás, A. G. Császár *et al.*, *J. Mol. Spectrosc.* **362**, 69 (2019).
- ¹⁴³L. K. McKemmish, A.-M. Syme, J. Borsovszky, S. N. Yurchenko, J. Tennyson, T. Furtenbacher, and A. G. Császár, *Mon. Not. R. Astron. Soc.* **497**, 1081 (2020).
- ¹⁴⁴T. Furtenbacher, T. Szidarovszky, C. Fábri, and A. G. Császár, *Phys. Chem. Chem. Phys.* **15**, 10181 (2013).
- ¹⁴⁵T. Furtenbacher, T. Szidarovszky, E. Mátyus, C. Fábri, and A. G. Császár, *J. Chem. Theor. Comput.* **9**, 5471 (2013).
- ¹⁴⁶K. L. Chubb, O. Naumenko, S. Keely, S. Bartolotto, S. MacDonald, M. Mukhtar, A. Grachov, J. White, E. Coleman, A. Liu, A. Z. Fazliev, E. R. Polovtseva, V.-M. Horneman, A. Campargue, T. Furtenbacher, A. G. Császár, S. N. Yurchenko, and J. Tennyson, *J. Quant. Spectrosc. Radiat. Transfer* **218**, 178 (2018).
- ¹⁴⁷R. Tóbiás, T. Furtenbacher, A. G. Császár, O. V. Naumenko, J. Tennyson, J.-M. Flaud, P. Kumar, and B. Poirier, *J. Quant. Spectrosc. Radiat. Transfer* **208**, 152 (2018).
- ¹⁴⁸A. R. Al Derzi, T. Furtenbacher, J. Tennyson, S. N. Yurchenko, and A. G. Császár, *J. Quant. Spectrosc. Radiat. Transfer* **161**, 117 (2015).
- ¹⁴⁹K. L. Chubb, M. Joseph, J. Franklin, N. Choudhury, T. Furtenbacher, A. G. Császár, G. Gaspard, P. Oguoko, A. Kelly, S. N. Yurchenko, J. Tennyson, and C. Sousa-Silva, *J. Quant. Spectrosc. Radiat. Transfer* **204**, 42 (2018).
- ¹⁵⁰T. Furtenbacher, P. A. Coles, J. Tennyson, S. N. Yurchenko, S. Yu, B. Drouin, R. Tóbiás, and A. G. Császár, *J. Quant. Spectrosc. Radiat. Transfer* **251**, 107027 (2020).
- ¹⁵¹C. Fábri, E. Mátyus, T. Furtenbacher, L. Nemes, B. Mihály, T. Zoltáni, and A. G. Császár, *J. Chem. Phys.* **135**, 094307 (2011).
- ¹⁵²M. S. Child and L. Halonen, *Adv. Chem. Phys.* **57**, 1 (1984).
- ¹⁵³M. Carleer, A. Jenouvrier, A.-C. Vandaele, P. F. Bernath, M. F. Mérienne, R. Colin, N. F. Zobov, O. L. Polyansky, J. Tennyson, and V. A. Savin, *J. Chem. Phys.* **111**, 2444 (1999).
- ¹⁵⁴A. Campargue, S. Kassi, A. Yachmenev, A. A. Kyuberis, J. Küpper, and S. N. Yurchenko, *Phys. Rev. Res.* **2**, 023091 (2020).
- ¹⁵⁵A. Campargue, A. M. Solodov, A. A. Solodov, A. Yachmenev, and S. N. Yurchenko, *Phys. Chem. Chem. Phys.* **22**, 12476 (2020).
- ¹⁵⁶R. A. Toth, SISAM database, <https://mark4sun.jpl.nasa.gov/h2o.html>, 2005.
- ¹⁵⁷R. J. Barber, J. Tennyson, G. J. Harris, and R. N. Tolchenov, *Mon. Not. R. Astron. Soc.* **368**, 1087 (2006).
- ¹⁵⁸O. L. Polyansky, A. A. Kyuberis, N. F. Zobov, J. Tennyson, S. N. Yurchenko, and L. Lodi, *Mon. Not. R. Astron. Soc.* **480**, 2597 (2018).
- ¹⁵⁹E. Mátyus, C. Fábri, T. Szidarovszky, G. Czákó, W. D. Allen, and A. G. Császár, *J. Chem. Phys.* **133**, 034113 (2010).
- ¹⁶⁰J. Smydke and A. G. Császár, *Mol. Phys.* **117**, 1682 (2019).
- ¹⁶¹M. S. Child, T. Weston, and J. Tennyson, *Mol. Phys.* **96**, 371 (1999).
- ¹⁶²A. G. Császár, W. D. Allen, and H. F. Schaefer III, *J. Chem. Phys.* **110**, 11971 (1999).
- ¹⁶³G. Tarczay, A. G. Császár, W. Klopper, V. Szalay, W. D. Allen, and H. F. Schaefer III, *J. Chem. Phys.* **110**, 11971 (1999).
- ¹⁶⁴E. F. Valeev, W. D. Allen, H. F. Schaefer III, and A. G. Császár, *J. Chem. Phys.* **114**, 2875 (2001).
- ¹⁶⁵S. V. Shirin, N. F. Zobov, R. I. Ovsyannikov, O. L. Polyansky, and J. Tennyson, *J. Chem. Phys.* **128**, 224306 (2008).
- ¹⁶⁶L. Lodi and J. Tennyson, *J. Quant. Spectrosc. Radiat. Transfer* **113**, 850 (2012).
- ¹⁶⁷P. Árendás, T. Furtenbacher, and A. G. Császár, *J. Math. Chem.* **54**, 806 (2016).
- ¹⁶⁸D. Wunch, G. C. Toon, J.-F. L. Blavier, R. A. Washenfelder, J. Notholt, B. J. Connor, D. W. T. Griffith, V. Sherlock, and P. O. Wennberg, *Philos. Trans. R. Soc. A* **369**, 2087 (2011).
- ¹⁶⁹H. Vogelmann, R. Sussmann, T. Trickl, and A. Reichert, *Atmos. Chem. Phys.* **15**, 3135 (2015).
- ¹⁷⁰E. Dupuy, I. Morino, N. M. Deutscher, Y. Yoshida, O. Uchino, B. J. Connor, M. De Mazière, D. W. T. Griffith, F. Hase, P. Heikkinen, P. W. Hillyard, L. T. Iraci, S. Kawakami, R. Kivi, T. Matsunaga, J. Notholt, C. M. Petri, J. R. Podolske, D. F. Pollard, M. Rettinger, C. Roehl, V. A. Sherlock, R. Sussmann, G. C. Toon, V. A. Velasco, T. Warneke, P. O. Wennberg, D. Wunch, and T. Yokota, *Remote Sensing* **8**, 414 (2016).
- ¹⁷¹C. Clerbaux, J. Hadji-Lazaro, S. Turquety, G. Mégie, and P.-F. Coheur, *Atmos. Chem. Phys.* **3**, 1495 (2003).
- ¹⁷²G. E. Nedoluha, R. Michael Gomez, D. R. Allen, A. Lambert, C. Boone, and G. Stiller, *J. Geophys. Res.: Atmos.* **118**, 11285 (2013).